

# Abbreviations and Notations

<b>ADC</b>	Analog-to-Digital Converter
<b>BER</b>	Bit Error Rate
<b>CP</b>	Cyclic Prefix
<b>CSI</b>	Channel State Information
<b>DAC</b>	Digital-to-Analog Converter
<b>EEP</b>	Equal Error Protection
<b>FFT</b>	Fast Fourier Transform
<b>ICI</b>	Intercarrier Interference
<b>IFFT</b>	Inverse Fast Fourier Transform
<b>ISI</b>	Intersymbol Interference
<b>MIMO</b>	Multiple-Input and Multiple-Output
<b>OFDM</b>	Orthogonal Frequency-Division Multiplexing
<b>PAPR</b>	Peak-to-Average Power Ratio
<b>SNR</b>	Signal-to-Noise Ratio
<b>STBC</b>	Space-Time Block Code
<b>STTC</b>	Space-Time Trellis Code
<b>UEP</b>	Unequal Error Protection

*Notation:* Upper (lower) bold face letters indicate matrices (column vectors). Superscript  $H$  denotes Hermitian,  $T$  denotes transposition,  $\dagger$  denotes the Moore-Penrose inverse.

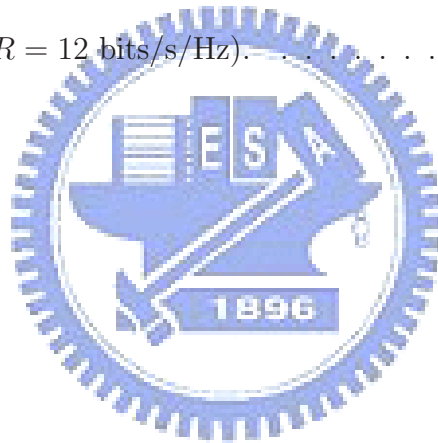
$E[\cdot]$  stands for statistical expectation of the entity inside the square bracket.  $E_x[\cdot]$  denotes for statistical expectation of the entity inside the square bracket with respect to the random variable  $x$ .  $\mathbf{I}_N$  denotes an  $N \times N$  identity matrix;  $\mathbf{0}_{M \times N}$  denotes an  $M \times N$  all zero matrix.  $[\mathbf{A}]_{ii}$  denotes the  $i^{\text{th}}$  diagonal element of the matrix  $\mathbf{A}$ .  $tr(\cdot)$  is the trace operator.  $\sigma_i(\mathbf{A})$  is the  $i^{\text{th}}$  singular value of  $\mathbf{A}$  arranged in descending order.  $\lfloor x \rfloor$  denotes the largest integer that is less than or equal to  $x$ .  $\lceil x \rceil$  denotes the smallest integer that is larger than or equal to  $x$ .  $\text{mod}(x, y)$  is an operator which gives the remainder of  $x/y$ .



# List of Figures

1.1	Multipath effect in wireless channels. . . . .	2
2.1	Schematic of the proposed cross-layer design scheme with DOSSA system .	7
2.2	Overview of MIMO-OFDM systems . . . . .	9
3.1	The cross-layer design video transport model with resynchronization markers being shown in blue, and protocol headers being shown in red. . . . .	14
3.2	Schematic of the proposed cross-layer design scheme with DOSSA system .	15
3.3	Analytical evaluation of fragment error probability of OSSA with different pairs of the number of subcarriers selected and its corresponding FEC rate. $N_c = 64$ , $N_{cp} = 16$ , $M_{\text{ref}} = 4$ , $R_{\text{ref}} = 1/2$ , $k_c = 56$ , and $m = 8$ . . . . .	21
3.4	Comparison between the analytical results (solid lines) and simulation results (circles) for fragment error probability of OSSA with FEC coding. $N_c = 64$ , $N_{cp} = 16$ , $M_{\text{ref}} = 4$ , $R_{\text{ref}} = 1/2$ , $k_c = 56$ , and $m = 8$ . . . . .	22
3.5	$-\frac{P_i^{\ell}(K_i)}{\hat{K}_i}$ vs. $K_i$ : (a) $i = 1$ , (b) $i = 144$ . The slice in (a) is from I-frame. The slice in (b) is from P-frame. $N_c = 64$ and SNR = 8.5 dB. $\hat{K}_i$ denotes the set of the possible candidates for $K_i$ , given $\lambda$ in different interval. . . . .	23
3.6	Average PSNR vs. frame index performance for the CLDOSSA, the UEP OSSA, the EEP implementation of [1] and the EEP OSSA when transmit SNR = 8.5 dB. Frame index is from 1 to 24. . . . .	28

3.7	PSNR vs. transmit SNR performance for the CLDOSSA, the UEP OSSA, the EEP implementation of [1] and the EEP OSSA. PSNR is measured across the first 24 video frames. . . . .	29
3.8	PSNR vs. transmit SNR performance for the CLDOSSA, the UEP OSSA of different FEC rate set, and the EEP OSSA. PSNR is measured across the first 24 video frames. . . . .	30
4.1	Block diagram of proposed multimode precoding scheme. . . . .	36
4.2	BER vs. SNR performance for multimode and unimode schemes ( $R = 4$ bits/s/Hz). . . . .	46
4.3	BER vs. SNR performance between multimode, unimode, SC1 [2], and SC5 [3] schemes ( $R = 12$ bits/s/Hz). . . . .	48



# List of Tables

4.1	Number of multiplications and additions for the proposed multimode precoding schemes, the unimode precoding scheme in Section 4.4, and an MIMO-OFDM implementation of the SC5 scheme in [3]. . . . .	45
-----	--	----



# Chapter 1

## Introduction

### 1.1 Research Motivations and Contributions

The widespread use of camera-equipped mobile devices have fueled the growth of multimedia data transmission in the uplink as more people are willing to upload photos and video clips onto websites such as Flickr and YouTube at anytime and anywhere. This has operators scrambling to upgrade their infrastructure to handle such upsurge in data transmission as their equipment was traditionally designed to handle large volume of data in the downlink, but not the uplink. In addition, unlike previous WCDMA standards which delivers data via circuit switched network, newly proposed IEEE 802.16e or the soon to be released LTE standards being developed by the 3GPP standards body focus primarily on delivering packet data service. Moreover, these standards have promoted the use of orthogonal frequency division multiplexing (OFDM) modulation for transmission due to its implementation simplicity. Hence, maximizing capacity, QoS, and link reliability for OFDM based systems have become paramount issues in wireless video transmission.

Obtaining good performance for multimedia communications over wireless channels is a challenging task. Unlike wired channels which are stationary and predictable, statistical property of wireless channels can be quite nonstationary. Two types of propagation

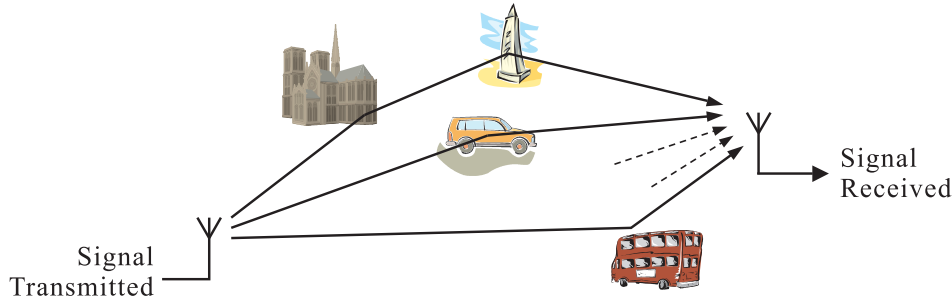


Figure 1.1: Multipath effect in wireless channels.

models are generally used to characterize wireless channels: large-scale model and small-scale/multipath fading model. Large-scale propagation is caused by path loss or shadowing, which usually fluctuates slowly and can be compensated by power control. Small-scale propagation is caused by the constructive and destructive interference produced by the multipath effect. Hence, small-scale propagation is also referred to as multipath fading, or simply fading. This is illustrated in Figure 1.1. The multipath effect greatly degrades the link reliability of transmission and causes high packet loss rate during multimedia data transmission over IP networks. This packet loss can cause unpleasant blocking effect and jerkiness in the received video signal.

Many source coding techniques have been proposed to circumvent these problems. For instance, in H.264/AVC codec, slicing and resynchronization marker (RM) have been used as a way to camouflage the effects of packet loss. With slicing, one video frame can be transmitted with multiple packets containing the data of slices over the IP networks. This enables partial frame recovery by the decoder despite the loss of slices in the video frame. Although such techniques have worked relatively well in static channels, performance can degrade rapidly when channel estimates become inaccurate, which happens quite frequently when coherence time of the channel is relatively small compared to the transmit symbol period. Moreover, transmitting multimedia data such as video is different from regular data transmission as video has different delay requirement compared to regular data.

Methods to alleviate has been partly hampered by the Open Systems Interconnection (OSI) 7-layer model [4]. This model attempts to abstract common features that are common to all approaches in data communications and organize them into layers or modules such that design of each layer is dependent only on the input and output parameters of the layer directly above and below it. This alleviates designers of the intricacy of the other layers. This model has worked well in the past when the parameters of the communication link remained static, which is not the case for wireless communications. As a result, suboptimal performance is often encountered when systems based on this model are deployed. This has led to the development of cross-layer design, which if designed appropriately, can lead to increased transmission efficiency and reliability.

Based on this concept, a cross-layer dynamic subcarrier selection algorithm (CLDOSSA) is proposed to dynamically determine the number of subcarriers to be employed in OFDM based systems so that unequal error protection (UEP) can be offer to minimize the end-to-end video distortion. Simulation results in Chapter 3 will show that the proposed method outperforms other OSSA methods in terms of video quality.

Further gain in link reliability and capacity can be attained by deploying multiple antennas in OFDM based systems [5]. This is commonly known as multiple-input multiple-output OFDM or MIMO-OFDM. This is an attractive alternative as significant capacity and diversity gain in frequency-selective fading channels can be achieved without sacrificing spectral efficiency nor incurring heavy computational burden. Exploiting the dynamic subcarrier allocation concept developed in Chapter 3, a bit error rate (BER) optimized multimode MIMO antenna selection/precoding design is proposed for MIMO-OFDM based spatial multiplexing systems in Chapter 4 where spectral and spatial resources at the transmitter are dynamically allocated<sup>1</sup> according to channel state information (CSI) to achieve high link reliability such that even higher video fidelity can

---

<sup>1</sup>Unimode antenna selection schemes, on the other hand, only entail selection of the antenna subset



be obtained at the receiver when packetized video are transmitted. The proposed design does not require the use of optimal but computational expensive maximum-likelihood receivers to achieve higher diversity gain than other similar antenna selection techniques.

## 1.2 Thesis Organization

This thesis mainly concerns with the design of resource allocation algorithms which take into account dynamic nature of system to enhance system performance.

- A description of the system model for OFDM and MIMO-OFDM based systems will be given in Chapter 2. This is followed by a brief review of video transmission fundamentals.
- Detailed formulation and simulation results of the CLDOSSA will be given in Chapter 3.
- In Chapter 4, a detail formulation and simulation results of the BER optimized multimode precoder design will be given.
- Finally, conclusion and future work will be discussed in Chapter 5.



## 1.3 Publications

Journal Publications:

**C.-H. Chen**, C.C. Fung, and S.-J. Wang, “Cross-Layer Dynamic Ordered Subcarrier Selection Algorithm for OFDM Based Video Transmission” *in preparation*.

**C.-H. Chen**, C.C. Fung, and S.-J. Wang, “BER Optimized Multimode Precoder Design for MIMO-OFDM Based Spatial Multiplexing Systems” *in preparation*.

Conference Publications:

**C.-H. Chen**, C.C. Fung, and S.-J. Wang, “Packetized Video Transmission for OFDM

Wireless Systems with Dynamic Ordered Subcarrier Selection Algorithm,” *in Proc. IEEE Int. Conf. Acoustics, Speech and Signal Processing*, Apr. 2009.

**C.-H. Chen**, C.C. Fung, and S.-J. Wang, “BER Optimized Unimode Precoder Design for MIMO-OFDM Based Spatial Multiplexing Systems,” *to be submitted to the IEEE Conf. on Communications*, May. 2010.



# Chapter 2

## Background

### 2.1 OFDM Basics

OFDM have been used or proposed to be used extensively in a variety of wireless communication systems because of its ability to achieve high data rate using low-complexity transceiver. The system model of OFDM is illustrated in Figure 2.1. The data symbols are modulated and converted to block symbols. Inverse fast Fourier transform (IFFT) is performed to the block symbols to impose the orthogonality among subcarriers. Samples at the output of the IFFT block are converted from parallel to serial data symbols and transmitted over the channel. Assuming the channel is frequency-selective, in order to counter the intersymbol and intercarrier interference (ISI and ICI), a guard interval in the form of cyclic prefix (CP) is added to each OFDM symbol before data transmission. At the receiver, the reverse process is performed to demodulate the data symbol. Since the OFDM symbol time is relatively long compared to the channel time characteristics, the effect of ISI can be eliminated when sufficient CP is added. Hence, each subcarrier can be regarded as flat-fading channel. Thus, the design of equalizer for OFDM based systems can be greatly simplified compared to its single subcarrier counterparts. Given all these benefits, there are disadvantages of OFDM systems. The link reliability of OFDM based

systems can greatly degrade due to ICI incurred by doppler shift or frequency synchronization problem. A higher number of subcarriers will also increase the Peak-to-Average Power Ratio (PAPR); demanding the use of linear and consequently inefficient power amplifiers. Moreover, the transmission efficiency is reduced due to the insertion of CP. Although link reliability degradation due to deep fades can be combated with channel coding and interleaving, this will also reduce spectrum efficiency of the system.

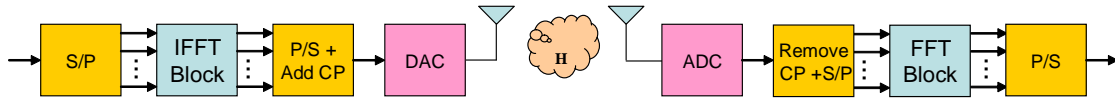


Figure 2.1: Schematic of the proposed cross-layer design scheme with DOSSA system

## 2.2 Single-User MIMO and MIMO-OFDM

The invention of single-user MIMO (SU-MIMO)<sup>1</sup> has brought tremendous changes over the last decade in the wireless communications community. This is understandable as MIMO has the potential to offer spatial multiplexing and spatial diversity gain, which leads to increases in data rate, link reliability, and transmission range without sacrificing spectrum efficiency [6, 7]. The major tradeoff is an increase in hardware complexity.

With spatial multiplexing, the bandwidth efficiency can be greatly increased by sending multiple data streams with multiple antennas in parallel. This can theoretically increase the capacity by a factor of  $\min(N_t, N_r)$ , where  $N_t$  and  $N_r$  denote the number of transmit and receive antennas, respectively. Diversity gain can be realized via space-time block coding (STBC) and space-time trellis coding (STTC), which impose redundancy in

<sup>1</sup>To be referred simply as MIMO henceforth. In this work, only SU-MIMO systems are dealt with as multiuser MIMO systems have different limitations and performance compared to SU-MIMO systems.

the data across time and space. However, there exists a fundamental tradeoff between these two gains such that they cannot be simultaneously optimized [8]. Furthermore, this theoretical gain is only possible under the assumption that the channel is spatially uncorrelated, which is not the case when the transceiver is operating in a poor scattering environment or when the antenna spacing is insufficient.

Antenna subset selection has become a viable solution to tackle this problem. This involves selection of reliable transmit and/or receive antennas with the objective of either boosting the data rate or link reliability. Several prior works, such as [2] and [3], have been in this area. [2] has proposed selection criteria based on the post-processing gain at the receiver to select reliable transmit antenna and reduce the channel co-interference among transmit antennas by selecting a subset of antennas. [3] take into account the constellation as well as the number of antennas employed among all the transmit antennas to further exploit spatial diversity.

Since most studies of MIMO systems have only consider flat-fading channels, it is natural to combine OFDM and MIMO technologies so that the effects of frequency-selective fading channels can easily be dealt with while sustaining high data. Block diagram of a MIMO-OFDM system is shown in Figure 2.2. The DAC and ADC blocks are ignored in the figure for simplification. Even though each subcarrier of an MIMO-OFDM system can be regarded as a MIMO flat-fading channel due to the orthogonality amongst the subcarriers, antenna selection methods designed for MIMO systems cannot be simply extended to MIMO-OFDM systems as it does not take into account the extra design freedom offered by MIMO-OFDM. The results in Chapter 4 will verify this fact and will show that with proper design of the selection algorithm, tremendous performance gain can be achieved.

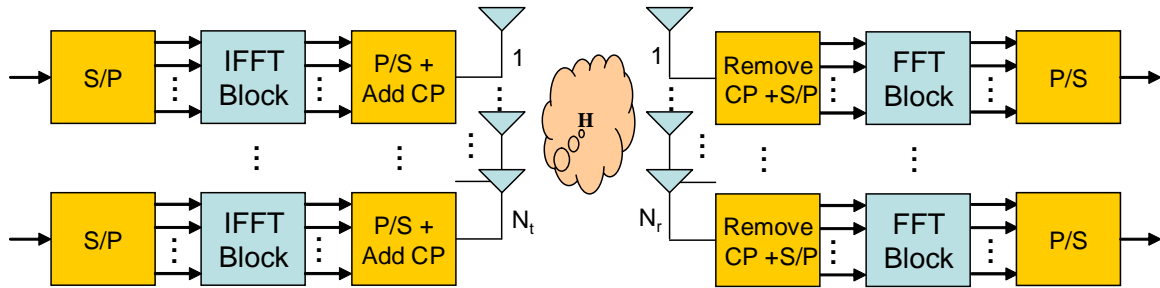


Figure 2.2: Overview of MIMO-OFDM systems

## 2.3 Fundamentals of Video Transmission

Slicing and resynchronization marker (RM) have been used to combat the adverse effects brought about by transmitting through a harsh wireless environment. A slice contains a group of macroblocks (MBs), and each slice is independently decodable. RM is a set of prefixed bits in each slice that is used at the decoder to achieve resynchronization even if the previous slice is lost or corrupted beyond repairs. It contains information about the slice such as number of MBs encoded and the position of MBs in the video frame.

Slices are appended with protocol headers and packetized into network layer packets and fragmented into link-layer fragments. Protection of each of the fragments can be done via the use of forward error codes (FEC), so that the fragment error rate can be controlled via adjustments in the FEC rate. These fragments are passed to the physical layer before being launched over the wireless channel. At the receiver, the source decoder can only decode error-free slices and discard slices with bit errors.

# Chapter 3

## Cross-Layer Design for OFDM Based Video Streaming Systems

### 3.1 Overview

Multicarrier systems, such as Orthogonal Frequency Division Multiplexing (OFDM), have been used extensively in a variety of wireless communications protocols because of its ability to achieve high data rate using low complexity transceiver. This has proliferated video communications using mobile devices, making it possible to send high quality video at anytime and anywhere.

In packet based wireless video transmission, the video is first compressed and then packetized before it is transmitted across the fading channel. Besides utilizing error concealment techniques at the source coder, the design of the transmission algorithm also plays a crucial role in increasing reliability, as well as throughput, of the transmitted data. Traditionally, the task of designing the source coder and transmission scheme can remain separate due to the abstraction provided by the Open Systems Interconnection (OSI) 7-layer model [4]. This model attempts to abstract common features that are common to all approaches in data communications and organize them into layers or modules such that

design of each layer is dependent only on the input and output parameters of the layer directly above and below it. This alleviates designers of the intricacy of the other layers. This model has worked well in the past when the parameters of the communication link remain static, which is not the case for mobile communications. As a result, suboptimal performance is often encountered when systems based on this model are deployed. This has led to the development of cross-layer design, which if designed appropriately, can lead to increased transmission efficiency and reliability.

Several cross-layer design schemes have recently been proposed for video transmission using OFDM. For example, [9] grouped the subcarriers selected by the Ordered Subcarrier Selection Algorithm (OSSA) [10] to form number of subchannels and exploited unequal error protection (UEP) at the modulation level by assigning the layered video (MPEG-4) of high importance to high quality subchannels. However, there is no optimization for the grouping of subchannels and the assignment of subchannel to a corresponding video layer. [11] further extended [9] to jointly optimize the diversity of channel gain among different subcarriers, which are selected by the OSSA, channel coding rates and subchannel assignment for layered video of different importance. Both of these schemes are based on the layered video framework and benefit from the characteristic of the OSSA that can provide better link reliability by selecting the top strongest subcarriers for data transmission; allowing it to offer UEP for different data. The advantage of the OSSA is that it has low implementation complexity due to the fact that power allocation and bit-loading are uniform across all the selected subcarriers. Moreover, since the OSSA requires only coarse channel state information (CSI) compared to other adaptive bit-loading algorithms or waterfilling based power allocation algorithms, the impact of delayed CSI feedback is alleviated. However, it does not guarantee an efficient usage of channel capacity and it cannot tradeoff between link reliability and transmission rate, which is important for video transmissions.



The CLDOSSA (Cross-layer dynamic ordered subcarrier selection algorithm) for packetized video transmission is proposed herein to tackle such a problem. The CLDOSSA tradeoffs link reliability and transmission rate by taking into account the content of the transmitted data. This is achieved by relaxing the constraint in the OSSA that a fixed number of selected subcarriers for data transmission has to be used. Based on this premise, a cross-layer design approach is presented to dynamically assign the number of selected subcarriers during video transmission according to the importance of the content. The dynamic assignment is formulated such that UEP can be offered to packet of different importance so that end-to-end video distortion is minimized. Moreover, the present scheme extends that of [12] where the selected subcarriers and the rate of forward error correction (FEC) coding performed at the link layer are jointly optimized. Furthermore, a more efficient technique of solving the optimization problem at hand compared to that of [12] is presented. The proposed scheme will be compared with the equal error protection (EEP) OSSA, OSSA with UEP at the link layer level using FEC, and the optimal bit/power loading algorithm for OFDM based systems proposed by [1].

This chapter is organized as follows. The system model for the OFDM-based video transmission system will be presented in Section 3.2. A detailed description of the proposed CLDOSSA will be given described in Section 3.3, followed by simulation results in Section 3.4.

## 3.2 Source Coding and Video Transport

Importance of the video content plays a significant role in the CLDOSSA in which it decides the number of subcarriers and FEC rate to be used. The video is encoded using H.264/AVC [13, 14]. The video sequences are encoded with group of pictures (GOP) structure, and there are  $N_s$  slices in a GOP. Each slices in the GOP is ordered with index  $i$  from the first video frame to the last video frame. The encoder is assumed to have full

knowledge of the error concealment scheme utilized at the receiver, so the transmitter can estimate the distortion resulting from the slice loss during video transmission.

Slicing and resynchronization marker (RM) are used to make the video more resistant to transmission error [15]. A slice contains a group of macroblocks (MBs), and each slice is independently decodable. RM is a set of prefixed bits in each slice that is used at the decoder to achieve resynchronization even if the previous slice is lost or corrupted beyond repairs. The RM also contains information about the slice, such as number of MBs encoded and the position of MBs in the video frame.

The expected decoder side distortion model proposed in [15, 16] is adopted in the present scheme to measure the importance of the video content. From [15], the expected value of the distortion at the decoder for the  $i^{th}$  slice is

$$E[D_i] = P_i^\ell D_i^C \gamma + (1 - P_i^\ell) D_i^Q, \quad (3.1)$$

where  $D_i^C$  is the concealment distortion if the  $i^{th}$  slice is not successfully received,  $D_i^Q$  is the quantization distortion if the  $i^{th}$  slice is perfectly received, and  $\gamma$  is the error propagation factor which accounts for the distortion caused by the loss of packets. The value of  $\gamma$  is set to the number of frames before the arrival of the next intrarefresh frame.  $P_i^\ell$  is the probability of the  $i^{th}$  slice loss, which will be derived in Section 3.3. Note that the decoder can only decode error-free slices, while the rest are simply discarded.

In the present scheme, it is assumed that transmission of the coded video is done by packetizing several H.264 slices into one packet. After packetization, the packet is sent to the link layer where further protection to the data can be provided in the form of FEC. The correction capability of the code can be controlled by adjusting the coding rate  $R_c$ . In order to offer better error resiliency to the video content transmitted over the wireless channel, the present scheme adopted the link layer strategy used in [15] in which the link layer frames are broken up into different fragments; with each fragment encoded with an FEC of the same rate as other fragments. In other words, each fragment

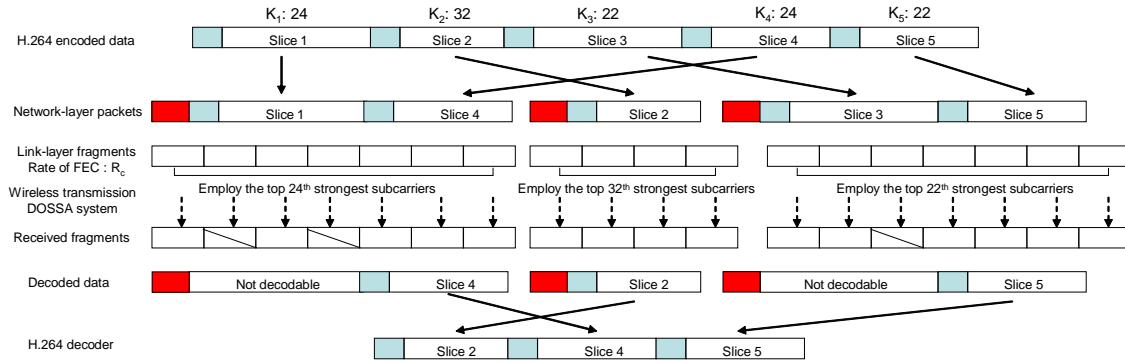


Figure 3.1: The cross-layer design video transport model with resynchronization markers being shown in blue, and protocol headers being shown in red.

is equally protected against transmission errors. However, in the proposed CLDOSSA, UEP is provided by varying the number of subcarriers being used for transmitting slices of different importance. This is shown in Figure 3.1, and Figure 3.2 gives the block diagram of the proposed cross-layer design video transport model.

### 3.3 Proposed CLDOSSA

The proposed CLDOSSA exploits the content information available in the application layer to jointly optimize the number of subcarriers  $K$  and the FEC rate  $R_c$  in order to minimize the average end-to-end video distortion while keeping the power allocation uniform across the selected subcarriers. Unlike the OSSA, where the optimal number of subcarriers are fixed to be

$$K_{\text{opt}} = \frac{N_c \log_2(M_{\text{ref}})}{\log_2(4M_{\text{ref}})}, \quad (3.2)$$

with  $M_{\text{ref}}$  defined as the modulation level for a reference OFDM system that uses all  $N_c$  subcarriers [10],  $K_{\text{opt}}$  for the proposed CLDOSSA scheme will be different for different segments of the video.

Since FEC coding performed in the link layer is assumed to be fixed for all the slices in the CLDOSSA, the slice error probability  $P_i^\ell$  in (3.1) will depend on the number of selected

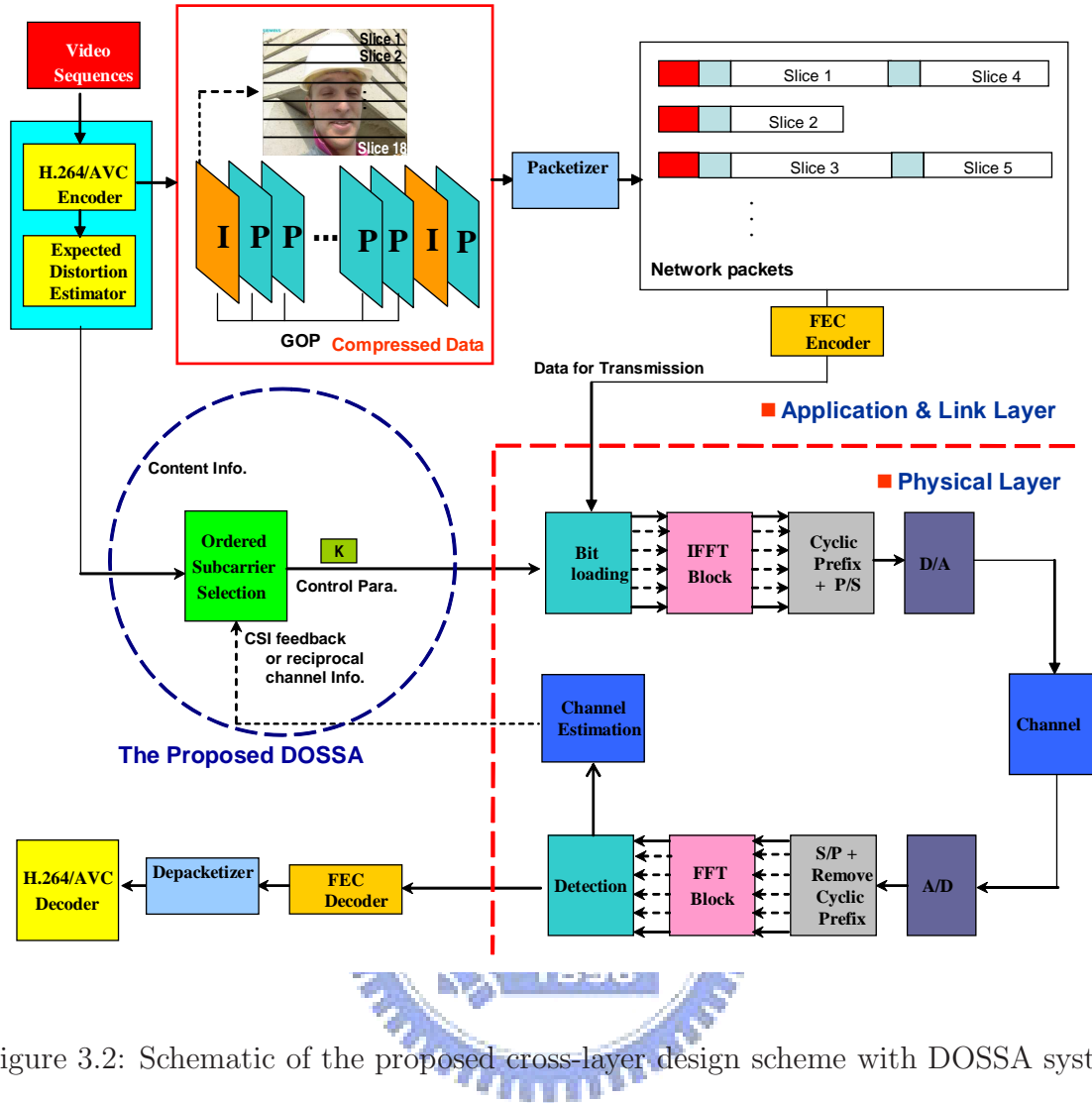


Figure 3.2: Schematic of the proposed cross-layer design scheme with DOSSA system

subcarriers  $K$  employed for transmission. The expected value of the video distortion for the  $i^{\text{th}}$  slice in (3.1) can be rewritten as

$$E[D_i(K)] = P_i^\ell(K) D_i^C \gamma + (1 - P_i^\ell(K)) D_i^Q \quad (3.3)$$

In order to minimize the end-to-end video distortion in a GOP, the modulation order  $M$ , FEC coding rate  $R_c$ , and the number of selected subcarriers  $K$  for different slices in a GOP can be jointly determined by solving

$$\begin{aligned}
& \min_{M, R_c, \mathbf{k}} \sum_{i=1}^{N_s} E[D_i(K_i)] \\
& \text{s.t.} \quad \sum_{i=1}^{N_s} r_i/K_i \leq \frac{1}{K_{\text{ref}}(M, R_c)}, \quad \text{for } 1 \leq K_i \leq N_c, K_i \in \mathbb{Z},
\end{aligned} \tag{3.4}$$

where  $\mathbf{k} = [K_1, K_2, \dots, K_{N_s}]^T$  is a column vector containing  $K_i$  for all the corresponding slices in the GOP, and  $r_i = N_i/(\sum_{j=1}^{N_s} N_j)$  is the size ratio of the  $i^{\text{th}}$  slice in the GOP. From (3.2), it is clear that

$$K_{\text{ref}}(M, R_c) = \frac{N_c \log_2(M_{\text{ref}}) R_{\text{ref}}}{\log_2(M) R_c} \tag{3.5}$$

denotes the number of subcarriers selected in the OSSA when  $M$ -QAM modulation and FEC with code rate  $R_c$  are employed such that the transmission rate is the same as that of the reference OFDM system. Since the number of subcarriers used during transmission differs from slice to slice in the CLDOSSA, the average number of subcarriers selected in the DOSSA is defined as  $K_{\text{avg}} \triangleq (\sum_{i=1}^{N_s} r_i/K_i)^{-1}$ . Hence, the rate constraint function can be written as  $(K_{\text{avg}})^{-1} \leq (K_{\text{ref}}(M, R_c))^{-1}$ , which implies the overall transmission time of the CLDOSSA should not exceed that of the reference OFDM system using the OSSA. This is done in order to compare performance of the two systems in a fair manner.

To explicitly derive  $E[D_i(K)]$  for all  $K$ , analysis of the slice error probability  $P_i^\ell(K)$  in (3.3) will have to be carried out. Since each link layer fragment is encoded with linear Reed-Solomon block code  $\text{RS}(k_c, n_c, m)$  [17], where  $k_c$  denotes the number of information symbols to be encoded,  $n_c$  denotes the number of codeword symbols, and each symbol is made up of  $m$  bits, the slice error probability for the  $i^{\text{th}}$  slice can be formulated as  $P_i^\ell(K) = 1 - (1 - \overline{P}_{\text{ep}}(K))^{N_i}$ , where  $N_i = \left\lceil \frac{L_i}{m \cdot k_c} \right\rceil$  is the number of link layer fragments for the  $i^{\text{th}}$  slice.  $m \cdot k_c$  denotes the size of the fragments in terms of the number of bits, and  $L_i$  denotes the size of the  $i^{\text{th}}$  slice in terms of the number of bits.  $\overline{P}_{\text{ep}}(K)$  is the

link layer fragment error probability, which can be derived based on the method proposed in [10, 18] according to the ordering statistics of subcarrier selection. To analyze the link layer fragment error probability based on the linear Reed-Solomon block code, the codeword symbol error probability will have to be derived based on the average BER in the physical layer when different number of selected subcarriers are used for transmission.

It is assumed that the channel coefficients are generated independently with a Rayleigh distribution, the channel gain  $\lambda = |H_n|^2$ , for  $n = 1, 2, \dots, N_c$ , will consequently be exponentially distributed [17], so that  $f_\lambda(\lambda) = e^{-\lambda}$  and  $F_\lambda(\lambda) = 1 - e^{-\lambda}$  are the probability density and cumulative distribution function of the channel gain  $\lambda$ , respectively. Similar to [10], the subcarriers are first ordered based on its channel gain in ascending order such that  $\lambda_1 \leq \lambda_2 \leq \dots \leq \lambda_{N_c}$ , where  $\lambda_n = |H_{o(n)}|^2$  with  $o(n)$  being a function that returns the index of channel gains in ascending order. Hence, the probability distribution of the channel gain is [19]

$$\begin{aligned} f_n(\lambda_n) &= \frac{N_c! F_\lambda(\lambda_n)^{n-1} [1 - F_\lambda(\lambda_n)]^{N_c-n} f_\lambda(\lambda_n)}{(n-1)!(N_c-n)!} \\ &= \frac{N_c! e^{-\lambda_n(N_c-n+1)} (1 - e^{-\lambda_n})^{n-1}}{(n-1)!(N_c-n)!}, \quad \text{for } n = 1, 2, \dots, N_c. \end{aligned}$$

Assuming  $M$ -QAM modulation with Gray coding is employed for all subcarriers, the BER for the  $n^{\text{th}}$  subcarrier can thus be approximated as [10, 17]

$$P_{bn} \approx \frac{\sqrt{M} - 1}{\sqrt{M} \log_2 \sqrt{M}} \operatorname{erfc} \left( \sqrt{\frac{E_b}{N_0} \frac{3 \log_2(M) R_c \lambda_n \eta}{2(M-1)}} \right), \quad (3.6)$$

where  $R_c$  is the code rate of the FEC,  $\operatorname{erfc}(\cdot)$  is the complementary error function,  $E_b/N_0$  is the transmit SNR, and  $\eta \triangleq \frac{N_c}{N_c + N_{cp}}$  with  $N_{cp}$  denoting the length of the cyclic prefix.

Under the total transmission power constraint and the uniform power allocation over the selected subcarriers, the transmission power per bit in the proposed CLDOSSA is

$$E_b(K) = \frac{N_c \log_2(M_{\text{ref}}) R_{\text{ref}}}{K \log_2(M) R_c} E_b.$$

Replacing  $E_b$  with  $E_b(K)$  in (3.6), the BER expression for the  $n^{\text{th}}$  subcarrier can be

rewritten as

$$P_{b_n}(K) \approx \frac{\sqrt{M} - 1}{\sqrt{M} \log_2 \sqrt{M}} \operatorname{erfc} \left( \sqrt{\frac{N_c E_b}{K N_0} \frac{3 \log_2(M_{\text{ref}}) R_{\text{ref}} \lambda_n \eta}{2(M-1)}} \right). \quad (3.7)$$

Using  $f_n(\lambda_n)$ , the average BER can be written as

$$\bar{P}_{b_n}(K) = \int_0^\infty P_{b_n}(K) f_n(\lambda_n) d\lambda_n. \quad (3.8)$$

The closed-form expression for  $\bar{P}_{b_n}(K)$  can be derived according to [10], thus obtaining

$$\bar{P}_{b_n}(K) = \frac{N_c! (\sqrt{M} - 1)}{(n-1)! (N_c - n)! \sqrt{M} \log_2 \sqrt{M}} \sum_{i=0}^{n-1} \binom{n-1}{i} (-1)^i \frac{1 - \sqrt{\frac{b}{b + N_c - n + i + 1}}}{N_c - n + i + 1}, \quad (3.9)$$

where  $b = \frac{N_c E_b}{K N_0} \frac{3 \log_2(M_{\text{ref}}) R_{\text{ref}} \eta}{2(M-1)}$ .

To ease the derivation of codeword symbol probability, it is assumed that bits in the fragment are scrambled so that bits in the same codeword symbol are loaded into nonadjacent subcarriers so that each bit in the same codeword symbol is independent from each other. Hence, the codeword error probability for the  $i^{\text{th}}$  symbol can be represented as

$$\bar{p}s_i(K) = E_{\boldsymbol{\lambda}}[ps_i(K)] = 1 - \prod_{j=i \cdot m}^{(i+1) \cdot m - 1} (1 - \bar{P}_{b_{d(j)}}(K))$$

$$i = 0, 1, \dots, n_c - 1,$$

where  $\boldsymbol{\lambda} = \{\lambda_{N_c}, \lambda_{N_c-1}, \dots, \lambda_{N_c-K+1}\}$  denotes the channel realization when subcarrier selection is employed, and

$$d(j) = N_c - \operatorname{mod} \left( \left\lfloor \frac{I(j)}{\log_2(M)} \right\rfloor, K \right)$$

returns the index of the subcarrier in which the  $j^{\text{th}}$  coded bit is mapped.  $d(j)$  can be characterized by the permutation function

$$I(j) = \operatorname{mod}(j \sqrt{n_b}, n_b) + \left\lfloor \frac{j}{\sqrt{n_b}} \right\rfloor, \quad \text{for } j = 0, 1, \dots, n_b - 1,$$

where  $n_b = n_c m$  denotes the total number of bits in each fragment. It is assumed the codeword symbols are properly interleaved in different fragments so that each codeword symbol are independent from each other. The fragment error probability can thus be expressed as

$$\overline{P}_{\text{ep}}(K) = W(\overline{\text{ps}}(K); n_c, t), \quad (3.10)$$

where  $t$  denotes the error correction capability,  $\overline{\text{ps}}(K) = [\overline{ps}_0(K), \overline{ps}_1(K), \dots, \overline{ps}_{n_c-1}(K)]$  is a vector of average symbol error probabilities and  $W(\overline{\text{ps}}(K); n_c, t)$  is the probability that a number of errors larger than  $t$  are found in the first  $n_c$  code symbols and it can be recursively solved by the method proposed in [10].

Note that (3.4) is a nonlinear integer programming problem, thus, it is difficult to find the global optimum solution. However, a near-optimal solution can be found if  $M$  and  $R_c$  are eliminated from (3.4). This can be done by finding a suboptimal  $K_{\text{ref}}$ , denoted as  $K_{\text{ref}}^* = K_{\text{ref}}^*(M^*, R_c^*)$ , where  $M^*$  and  $R_c^*$  are optimal value of  $M$  and  $R_c$ , using (3.5). Recall from (3.2) that for square constellation such as  $M$ -QAM,  $K_{\text{opt}} \log_2(4M_{\text{ref}}) = N_c \log_2(M_{\text{ref}})$ . This implies that as  $K$  subcarriers are chosen from  $N_c$  number of subcarriers in an OSSA-OFDM based system, the modulation level has to be increased from  $M_{\text{ref}}$  to  $4M_{\text{ref}}$  in order for the OSSA-OFDM based system to have the same transmission rate as the reference OFDM system. From this, it can be concluded that  $M^* = 4M_{\text{ref}}$ .

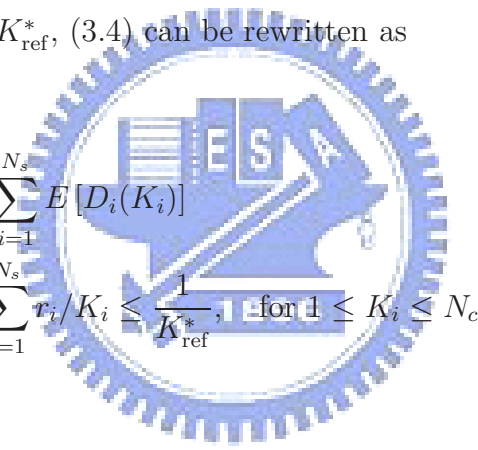
Substituting  $M^*$  into (3.5),

$$\begin{aligned} K_{\text{ref}}(M^*, R_c) &= \frac{N_c \log_2(M_{\text{ref}}) R_{\text{ref}}}{\log_2(M^*) R_c} \\ &= \frac{N_c \log_2(M_{\text{ref}}) R_{\text{ref}}}{\log_2(4M_{\text{ref}}) R_c} \\ &= K_* \end{aligned}$$

and (3.10) can be used to jointly determine  $K_*$  and  $R_c$  by considering a finite code rate set. Assuming packets of length  $k_c$  bytes are encoded with  $\text{RS}(k_c, k_c/R_c, m)$  and transmitted with  $K_*$  subcarriers. Denote  $(K_*, R_c)$  as a set of integer pairs consisting



of the number of subcarriers selected and its corresponding FEC rate. If  $N_c = 64$ ,  $N_{cp} = 16$ ,  $M_{\text{ref}} = 4$ ,  $R_{\text{ref}} = 1/2$ ,  $k_c = 56$ , and  $m = 8$ , then from (3.10),  $(K_*, R_c) = \{(20, 4/5), (24, 2/3), \dots, (44, 4/11), (48, 1/3)\}$ . Plotting the analytical average fragment error probability performance using the elements in  $(K_*, R_c)$  can then determine which pair renders the best performance. This is shown in Figure 3.3, which indicates that  $(24, 2/3)$  renders the best performance amongst all the elements in  $(K_*, R_c)$ . The simulated fragment error probability performance is also plotted in Figure 3.4 to verify the result in Figure 3.3. It is interesting to note that the optimal pair  $(24, 2/3)$  outperforms the coded OSSA in [10] when the optimal  $K$  and  $R_c$  are selected to be  $(32, 1/2)$ . After the optimal pair of  $K$  and  $R_c$ , denoted as  $(K^*, R_c^*)$ , has been found,  $K_{\text{ref}}^* = K_{\text{ref}}(M^*, R_c^*) = K^*$  is also determined. Using  $K_{\text{ref}}^*$ , (3.4) can be rewritten as



$$\begin{aligned} \min_{\mathbf{k}} \quad & \sum_{i=1}^{N_s} E[D_i(K_i)] \\ \text{s.t.} \quad & \sum_{i=1}^{N_s} r_i/K_i \leq \frac{1}{K_{\text{ref}}^*}, \text{ for } 1 \leq K_i \leq N_c, K_i \in \mathbb{Z}. \end{aligned} \quad (3.11)$$

Even though (3.11) is still a nonlinear, discrete constrained minimization problem, unlike the problem formulation in (3.4), a near-optimal solution for (3.11) can be easily found using Lagrangian relaxation [20], which is more efficient than the method proposed in [12]. Note that the feasible region for (3.11) is  $N_c^{N_s}$ , making exhaustive search infeasible. The Lagrangian relaxation of (3.11) with respect to the rate constraint is  $\ell_{LR}(\lambda) = \min_{\mathbf{k}} \ell(\mathbf{k}, \lambda)$ , for  $\lambda \in \mathbb{R}_+$ , where

$$\ell(\mathbf{k}, \lambda) = \sum_{i=1}^{N_s} E[D_i(K_i)] + \lambda \left( \sum_{i=1}^{N_s} r_i \tilde{K}_i - \frac{1}{K_{\text{ref}}^*} \right) \quad (3.12)$$

$$= \sum_{i=1}^{N_s} \left( E[D_i(K_i)] + \lambda \left( r_i \tilde{K}_i - \frac{1}{N_s K_{\text{ref}}^*} \right) \right) \quad (3.13)$$

$$= \sum_{i=1}^{N_s} \ell_i(K_i, \lambda), \quad \text{for } 1 \leq K_i \leq N_c, K_i \in \mathbb{Z},$$

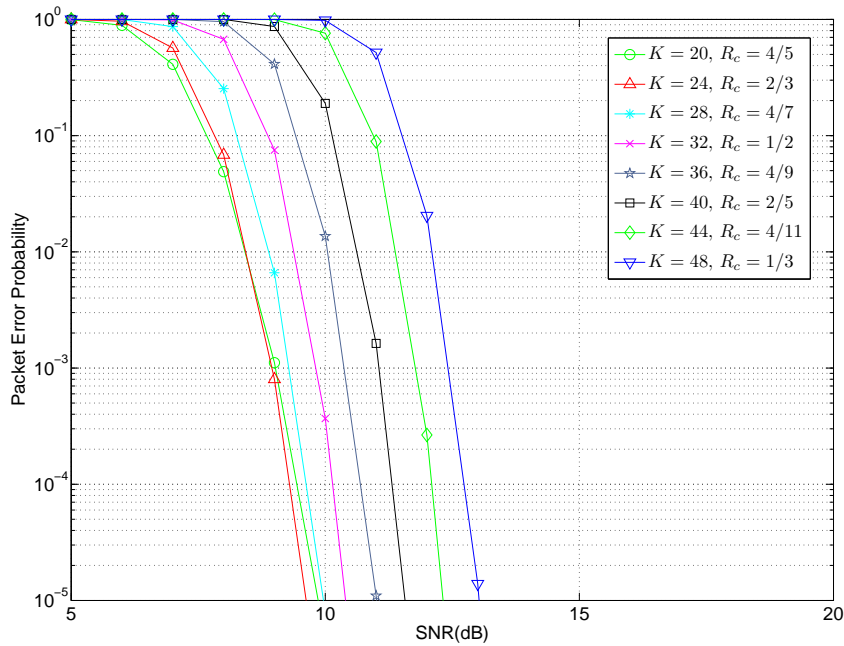


Figure 3.3: Analytical evaluation of fragment error probability of OSSA with different pairs of the number of subcarriers selected and its corresponding FEC rate.  $N_c = 64$ ,  $N_{cp} = 16$ ,  $M_{\text{ref}} = 4$ ,  $R_{\text{ref}} = 1/2$ ,  $k_c = 56$ , and  $m = 8$ .

is the Lagrangian with  $\tilde{K}_i \triangleq \frac{1}{K_i}$ . Note that  $\ell_i(K_i, \lambda)$  is the Lagrangian for the  $i^{\text{th}}$  slice. From the above, it is clear that  $\ell_i(K_i, \lambda)$  is independently additive since each slice is assumed to be independently decoded. As a result, the minima of  $\ell(\mathbf{k}, \lambda)$  is obtained when each  $\ell_i(K_i, \lambda)$  is minimized. Furthermore, the Lagrangian for all the slices share the same  $\lambda$ . Hence, once the optimal  $\lambda$  is known,  $\mathbf{k}$  can be determined by considering  $K_i$ , for  $i = 1, 2, \dots, N_s$ , which minimizes  $\ell_i(K_i, \lambda)$ .

According to the property of Lagrangian relaxation, the Lagrangian dual

$$\ell_{LD} = \max_{\lambda \geq 0} \ell_{LR}(\lambda) \quad (3.14)$$

will always lower bound the optimal solution for (3.11). Since  $\ell_{LR}(\lambda)$  is a piecewise linear and convex function of  $\lambda$ ,  $\ell_{LD}$  can be solved using the subgradient algorithm [20]. Furthermore, the near-optimal solution  $\lambda^*$  and  $\mathbf{k}^*$  can be refined by the branch and bound

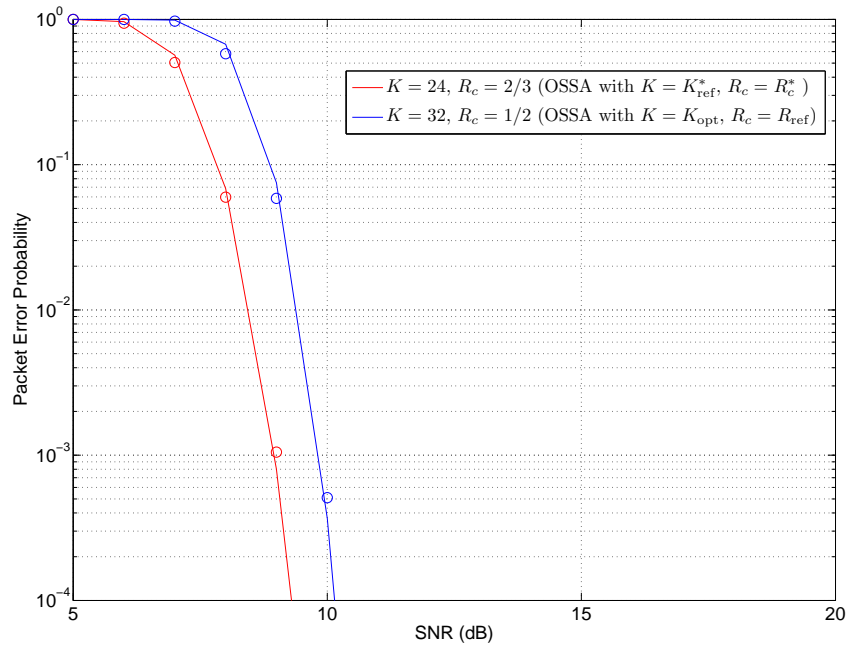


Figure 3.4: Comparison between the analytical results (solid lines) and simulation results (circles) for fragment error probability of OSSA with FEC coding.  $N_c = 64$ ,  $N_{cp} = 16$ ,  $M_{\text{ref}} = 4$ ,  $R_{\text{ref}} = 1/2$ ,  $k_c = 56$ , and  $m = 8$ .

algorithm [20] to obtain a better solution.

To iteratively obtain the near-optimal solution using subgradient algorithm, each iteration requires the computation of  $\ell_{LR}(\lambda)$ . Although the derivation of  $\mathbf{k}$  which minimizes  $\ell_{LR}(\lambda)$  can be simplified by solving each  $K_i$  that minimizes  $\ell_i(K_i, \lambda)$  for a given  $\lambda$  exhaustively, it may be computationally demanding as  $N_c N_s$  is large. However, a more computationally efficient searching method can be found by exploiting the convexity of  $\ell_i(K_i, \lambda)$  for different values of  $\lambda$ . The convexity of  $\ell_i(K_i, \lambda)$  can be deduced with the first-order condition of  $\ell_i(K_i, \lambda)$  so that possible candidates for  $K_i$  can be selected, and thus greatly reducing the searching space of  $K_i$ . Taking the first-order difference of (3.13) with respect to all  $K_i$ 's and setting the result to 0, we obtain

$$-\frac{P_i^{\ell'}(K_i)}{\tilde{K}_i'} \approx \lambda \frac{r_i}{(D_i^C \gamma - D_i^Q)}, \quad \forall i, \quad (3.15)$$

where  $P_i^{\ell'}(K_i)$  and  $\tilde{K}_i'$  denote the first-order difference of  $P_i^{\ell}(K_i)$  and  $\tilde{K}_i$ , respectively.

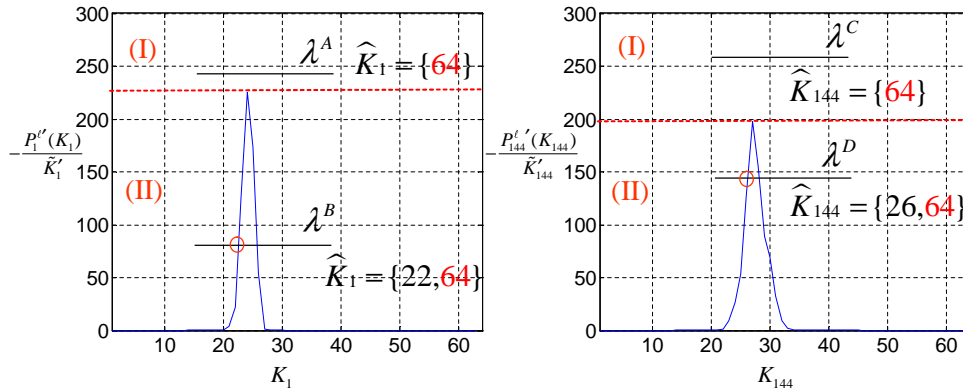


Figure 3.5:  $-\frac{P_i'(K_i)}{\tilde{K}_i}$  vs.  $K_i$ : (a)  $i = 1$ , (b)  $i = 144$ . The slice in (a) is from I-frame. The slice in (b) is from P-frame.  $N_c = 64$  and SNR = 8.5 dB.  $\hat{K}_i$  denotes the set of the possible candidates for  $K_i$ , given  $\lambda$  in different interval.

According to the number of suitable  $K_i$ 's that satisfy (3.15), given different values of  $\lambda$ , the vertical axis can be partitioned into two intervals of different types. A plot of  $-\frac{P_i'(K_i)}{\tilde{K}_i}$  vs.  $K_i$ , for  $i = 1$  and  $i = 144$  of the first GOP is shown in Figure 3.5. The convexity of  $\ell_i(K_i, \lambda)$  related to different types of interval of  $\lambda$  is indicated in Figure 3.5. In Type (I), there is no suitable  $K_i$  which satisfies (3.15), so no local minima nor maxima exist in  $\ell_i(K_i, \lambda)$ . In this case, the weighting on  $r_i \tilde{K}_i$  is relatively large such that  $\ell_i(K_i, \lambda)$  is dominated by  $r_i \tilde{K}_i$ .  $\ell_i(K_i, \lambda)$  becomes a convex function, so the extreme point  $N_c$  can be chosen as the optimal  $K_i$  which minimizes  $\ell_i(K_i, \lambda)$ . In Type (II), there are two suitable  $K_i$ 's that satisfy (3.15) which are denoted as  $K_i^L$  and  $K_i^R$ , where  $K_i^L < K_i^R$ . Since  $E[D_i(K_i)]$  is an increasing function and  $r_i \tilde{K}_i$  is a decreasing function with respect to  $K_i$ , it can be deduced that  $K_i^L$  is a local minimizer and  $K_i^R$  is a local maximizer. Nevertheless, the existence of the local maxima implies that the extreme point could also be the local minimizer. Therefore,  $K_i^L$  and  $N_c$  are both selected as possible candidates for  $K_i$ . Since there might be some error resulting from the approximation in (3.15), the selected  $K_i$  might not be exactly equal to the optimal  $K_i$  (but quite close to the optimal  $K_i$ ) which minimizes  $\ell_i(K_i, \lambda)$  the most. In order to deal with this problem, a possible

searching range centered at the possible candidates of  $K_i$  can be set up to enlarge the candidate set so that given a specified  $\lambda$ , a more accurate  $\mathbf{k}$  can be obtained. Since  $\lambda$  is a scalar, the subgradient algorithm can simply be implemented using the bisection method to obtain the solution efficiently. With the reduced search space of  $\mathbf{k}$ , a near-optimal solution for (3.11) can now be obtained efficiently by finding the smallest  $\lambda$  such that the corresponding  $\mathbf{k}$  satisfies the rate constraint in (3.11).

### 3.4 Simulation Results and Discussions

In all the simulations,  $N_c = 64$  and  $N_{cp} = 16$ . In this case,  $\eta = 0.8$ . A bandwidth of 20 MHz was employed. The channel coefficients are directly generated in the frequency domain with Rayleigh distribution. It is assumed that sufficient number of cyclic prefix symbols has been added to the system so that no ISI and ICI are incurred. The channel is assumed to be static during the transmission of link layer fragments. The modulation and FEC rate for the reference system are  $M_{\text{ref}} = 4$  and  $R_{\text{ref}} = 1/2$ , respectively. The transmission rate of the OSSA and DOSSA systems is the same as that of the reference system.

The video sequence used in the simulation is the first 24 frames of a video sequence “Stefan” in CIF (352x288 pixels) format and is encoded in the H.264 standard [14] with the baseline profile. There are 8 frames in a GOP. In each GOP, the first frame is an I-frame, followed by 7 P-frames. These frames are encoded such that each slice only contains a single row of MBs. There are 18 slices per video frame (a typical MB contains 16x16 pixels). All slices are fragmented into link layer fragments with 56 bytes and are encoded with RS(56, 56/ $R_c$ , 8). There are no retransmissions involved and the error concealment scheme used in the decoder is a simple frame copy when the corresponding slice is lost. 16-QAM is employed for the DOSSA and OSSA systems. Based on the fragment error probability analysis derived in Section 3.3, the optimal selection of  $R_c$  and

$K_{\text{ref}}$  in the objective function are  $2/3$  and  $24$  respectively. Hence, the link layer fragments are encoded using a code rate of  $R_c = 2/3$  in the proposed CLDOSSA.

The algorithms proposed in [9, 11] were not used in our simulations for performance comparison with the proposed CLDOSSA because both approaches are based on layered video architecture, which is different from our packet-based video format. Hence, an UEP OSA and EEP OSA will be used to demonstrate the efficacy of the proposed scheme in a fair manner. Note that the UEP OSA used here is different from the one reported in [9] where UEP in [9] is provided via channel coding in the physical layer. The UEP OSA used here employs the OSA with link layer FEC where the FEC rate of each slice is controlled by the application layer to achieve UEP. This type of FEC coding scheme was also reported in [15] as *Model 2*. In the network layer, slices of the code rate will be packetized into the same packet appended with protocol header and passed to the link layer. The link layer frame will be fragmented into fragments and encoded using FEC with the assigned code rate. The OSA-OFDM based system will then transmit the encoded fragments. The difference between the proposed CLDOSSA and UEP OSA is that UEP in CLDOSSA is provided to different slices by employing different number of subcarriers for transmission under constant rate of FEC, while the number of subcarriers selected for the UEP OSA is same for all slices while the FEC rate for different slices is different. Note that the average code rate will be the same as that of the CLDOSSA. The assignment of the FEC rate for each slice in the UEP OSA-OFDM based system can be determined using a method similar to the one described in Section 3.3 to minimize the overall expected video distortion in a GOP. The probability of slice loss in the expected distortion function will be determined by the FEC rate employed for each slice based on the analysis of packet error rate in [10]. EEP OSA is simply an OSA based schemes that does not employ any cross-layer design techniques. Therefore, the number of subcarriers selected and the FEC performed in the link layer is assumed to

be static during the video transmission. In addition to the above OSSA based techniques, the optimal bit/power loading algorithm for multicarrier systems proposed by [1] will also be used for comparison. The algorithm in [1] can guarantee optimal bit loading as well as efficient power allocation to minimize BER using a greedy algorithm. Since the slice error probability for video transmission system utilizing this algorithm is intractable, only an EEP version of the algorithm will be used for comparison.

For ease of comparison, it is assumed that the available FEC rates for the UEP OSSA are  $\mathcal{R}_0 = \{1/2, 7/12, 2/3, 4/5, 7/8\}$ . According to the optimal  $K_{\text{ref}}$  and  $R_c$  derived in Section 3.3 for the coded OSSA, the average FEC rate for the UEP OSSA will be  $2/3$ , and the link layer fragments are transmitted over the top  $24^{\text{th}}$  strongest subcarriers. For the EEP implementation of [1], the FEC rate is the same as that of the reference OFDM based systems with  $R_c = 1/2$ . Also, it is assumed that the available constellation set are QPSK, 16-QAM, 64-QAM and 256-QAM. Furthermore, the EEP OSSA that employs  $K_{\text{ref}}^*$  and the corresponding  $R_c^*$ , and one which employs  $K_{\text{opt}}$  from (3.2) and  $R_{\text{ref}} = 1/2$  are also used for comparison.<sup>1</sup>

Figure 3.6 shows that video quality, in terms of average PSNR, of transmission systems employing the proposed CLDOSSA, UEP OSSA, EEP Campello and EEP OSSA. The transmit SNR is equal to 8.5 dB. It is clear that the CLDOSSA and UEP OSSA perform far better than the EEP OSSA in the first few frames of GOP. The video quality degrades due to the error propagation incurred by packet loss. Although the performance of the CLDOSSA degrades more rapidly than that of the EEP OSSA, the average PSNR is still higher than that of the EEP OSSA system, as shown in the figure. The average PSNR of the CLDOSSA is 5.5 dB better than that of the EEP OSSA and also outperforms the UEP OSSA and the EEP implementation of [1] by 2.6 dB and 1.7 dB, respectively. Figure 3.7 also shows that the CLDOSSA consistently outperforming the UEP OSSA and

---

<sup>1</sup> $R_{\text{ref}}$  is the FEC rate used in the reference OFDM based system.

EEP OSSA. Also, the EEP OSSA based system which employs the optimal  $K_{\text{ref}}$  and  $R_c$  outperforms the EEP OSSA based system that employs the  $K_{\text{opt}}$  and  $R_{\text{ref}}$ . This agrees with the simulation results of fragment error probability shown in Figure 3.4. Clearly, the proposed CLDOSSA is able to outperform the EEP OSSA in terms of PSNR because the CLDOSSA exploits knowledge about the video content; allowing it to better assign channel resources for video transmission. Moreover, the proposed CLDOSSA outperforms the UEP OSSA because the present scheme can offer a fine-grained level of UEP by directly accessing the control of data transmission in the physical layer. It can be observed from Figure 3.7 that [1] outperforms the CLDOSSA at high SNR. This performance gain comes at the cost of increased implementation complexity to support adaptive modulation. In addition, extra CSI feedback is needed by the algorithm in [1] to support adaptive power allocation and bit loading. At low SNR (less than 9 dB), it is obvious that the CLDOSSA outperforms [1] since the latter does not take content information into the account so that relative to the CLDOSSA, the video content of higher importance cannot be well protected.

In order to investigate what effect the FEC granularity have on the UEP OSSA, three different FEC rate sets are provided for comparison:  $\mathcal{R}_1 = \{14/27, 14/21, 14/15\}$ ,  $\mathcal{R}_2 = \{14/27, 14/24, 14/21, 14/18, 14/15\}$  and  $\mathcal{R}_3 = \{14/k \mid k = 47, 45, \dots, 17, 15\}$ . Figure 3.8 shows the video quality for the OSSA systems with different granularity of UEP levels, and the performance for the CLDOSSA and EEP OSSA are also plotted for reference. Even though the UEP OSSA with  $\mathcal{R}_2$  and  $\mathcal{R}_3$  can further improve the video quality of the UEP OSSA with  $\mathcal{R}_1$  by employing a more fine-grained level of UEP, the CLDOSSA still outperforms the UEP OSSA, especially at low SNR. When SNR is low, the CLDOSSA will employ less subcarriers and allocate power to those reliable subcarriers. This is similar to the concept of waterfilling based power allocation algorithms. Hence, OFDM based systems using the CLDOSSA has higher flexibility to make use of the channel compared



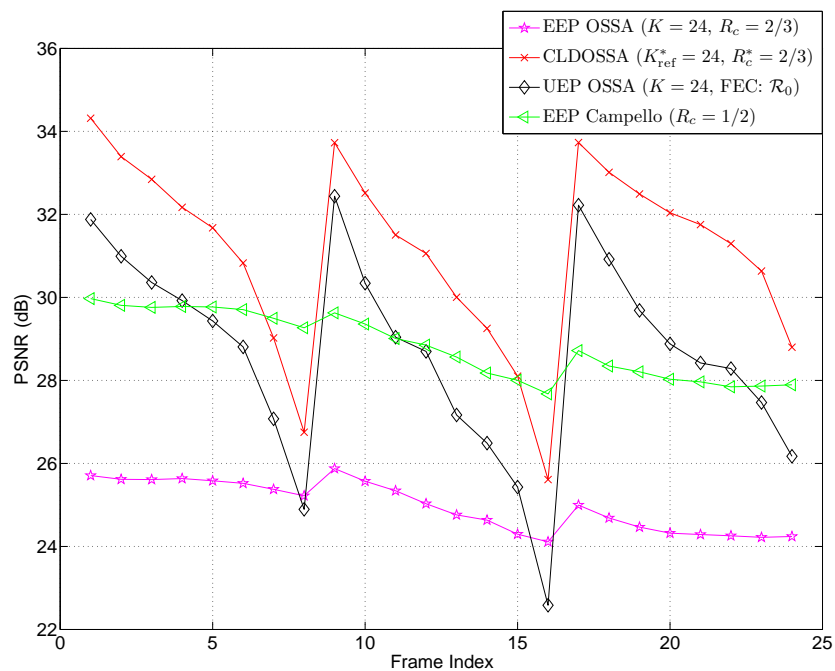


Figure 3.6: Average PSNR vs. frame index performance for the CLDOSSA, the UEP OSSA, the EEP implementation of [1] and the EEP OSSA when transmit SNR = 8.5 dB. Frame index is from 1 to 24.

to similar systems using the OSSA, and thus provide a wider range of UEP to protect important slices when channel is greatly attenuated.

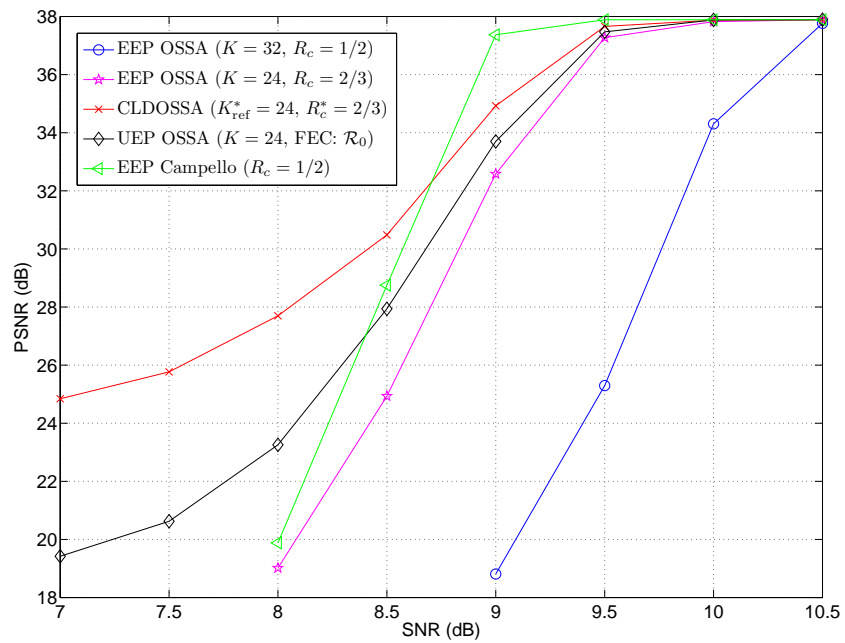


Figure 3.7: PSNR vs. transmit SNR performance for the CLDOSSA, the UEP OSSA, the EEP implementation of [1] and the EEP OSSA. PSNR is measured across the first 24 video frames.

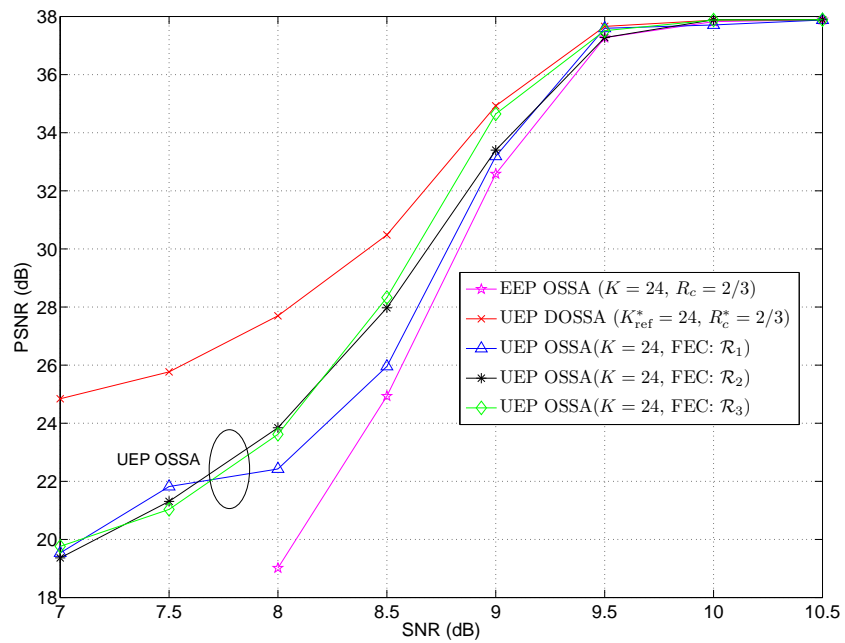


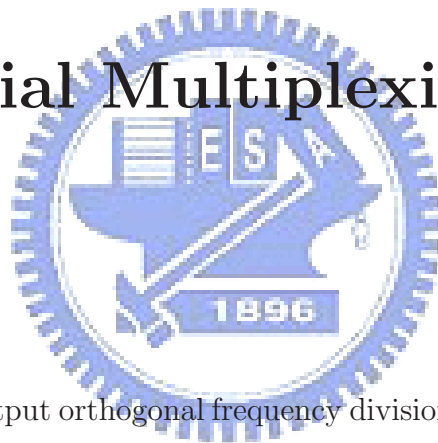
Figure 3.8: PSNR vs. transmit SNR performance for the CLDOSSA, the UEP OSSA of different FEC rate set, and the EEP OSSA. PSNR is measured across the first 24 video frames.

# Chapter 4

## BER Optimized Multimode

## Precoder Design for MIMO-OFDM

## Based Spatial Multiplexing Systems



### 4.1 Overview

Multiple-input multiple-output orthogonal frequency division multiplexing (MIMO-OFDM) has been extensively promoted as key technology for next generation of wireless communication systems due to its potential to achieve significant capacity and diversity gain in frequency-selective fading channels without sacrificing spectral efficiency nor incurring heavy computational burden [5]. This capacity gain can however be offset by spatial correlation among the antennas, especially at the mobile terminal where limited space imposes a severe constraint on the placement of the antennas.

Antenna selection has been proposed as an effective and inexpensive means to combat against this problem as it reduces the number of RF chains at the transceiver while retaining many of the diversity benefits. The selection procedure often relies on channel state information (CSI) feedback from the receiver to transmitter [21–23]. It was shown

in [24,25] that space-time coded (STC) MIMO-OFDM can attain full diversity of  $L_h N_t N_r$ , where each term is denoted as the channel length, number of transmit antenna, and number of receive antennas, respectively. [25] has further shown that employing antenna selection does not change this diversity advantage. This fact has motivated various selection schemes [26–29] for MIMO-OFDM based systems. [26] extended the maximum capacity unimode antenna selection scheme<sup>1</sup> in [23] to select a subset of the total number of transmit and receive antennas for transmission by successive eliminating the columns/rows of the channel matrix that yields the minimum loss in capacity. This scheme, however, does not yield the best bit error rate (BER) performance nor does it guarantee the maximum diversity order can be achieved. The multimode schemes in [27,29] exploit space-frequency block coding (SFBC), adaptive modulation, and an energy-based antenna selection scheme to further enhance performance. However, the methods do not guarantee optimal BER can be attained as the design scheme does not directly optimizes the BER expression. [28] proposed a minimum mean-squared error (MMSE) based selection scheme which utilized similar successive elimination concept as in [23,26]. However, it suffers from the same deficiency as [27,29] in terms of BER optimization. Furthermore, it is unclear what data rate each data stream should have after the selection has been done. While the above techniques assumed a fixed amount of antennas are to be selected, [30] relaxed this constraint and proposed a joint transmit and receive (Tx/Rx) MMSE selection scheme to reduce the BER. Significant improvements in BER performance was reported over conventional MMSE joint Tx/Rx design such as [31,32] which uses a fixed number of antennas. Unfortunately, the global optimal solution was found only via an exhaustive search. This was acceptable since [30] only considered flat fading MIMO channels with small number of antenna elements.

Herein, a multimode transmit antenna selection/precoding algorithm is proposed for

---

<sup>1</sup>Unimode antenna selection schemes only entail selection of the antenna subset.

MIMO-OFDM based spatial multiplexing systems. The proposed multimode precoding algorithm is designed to optimize average BER over all data streams under a constant rate constraint by 1) determining the necessary number of antennas/spatial streams and subcarriers that are needed, and 2) choosing the appropriate mapping of the data stream to the selected antennas and subcarriers for transmission. The present scheme is able to choose the strongest spatial and spectral channels such that the BER is minimized and can easily tradeoff between diversity and spatial multiplexing gain, as discussed in [8]. The other advantages of the proposed method include: 1) the use of linear receivers only, such as zero-forcing (ZF) or MMSE, for signal recovery, thus bypassing the use of computational expensive receivers such as maximum likelihood, and 2) the solution, although suboptimal, does not resort to performing exhaustive search. Results will show that the proposed method can outperform the multimode method proposed by [28] and the OFDM implementation of the multimode methods proposed by [2, 3]. Furthermore, our simulation results will indicate that increased diversity order can be achieved compared to those reported in [2, 3] by exploiting spatial and channel gain diversity since the number of antenna, number of subcarrier, and the mapping of the data stream to those selected antennas and subcarriers are adjusted adaptively based on CSI feedback.

This chapter is organized as follows. Section 4.2 describes the system and the data model. The proposed scheme is developed in Section 4.3, followed by a complexity analysis in Section 4.5. Simulations in Section 3.4 verify the efficacy of the proposed scheme.

## 4.2 System Model

Consider a MIMO-OFDM system with  $N_t$  transmit antennas,  $N_r$  receive antennas and  $N_c$  subcarriers. The data symbols of each antenna are modulated with  $M$ -QAM constellation and converted to block symbols. We assume the constellation is uniform over all the data streams of all the antennas. Inverse fast Fourier transform (IFFT) is performed to the

block symbols to impose orthogonality among subcarriers. Samples at the output of IFFT block are converted from parallel to serial data symbols and transmitted over frequency-selective fading channels. In order to counter intersymbol interference (ISI), a guard interval in the form of cyclic prefix of length  $N_{cp}$  is added to each OFDM symbol of length  $N_c$  before transmission. At the receiver, the reverse process is performed to demodulate the data symbol. The transmission efficiency due to the cyclic prefix is defined as

$$\eta \triangleq \frac{N_c}{N_c + N_{cp}}.$$

Each subcarrier can be regarded as an independent MIMO flat fading channel due to the orthogonality among subcarriers. The channel matrix  $\mathbf{H}(k)$  for the  $k^{th}$  subcarrier is

$$\mathbf{H}(k) = \begin{bmatrix} H_{1,1}(k) & H_{1,2}(k) & \cdots & H_{1,N_t}(k) \\ H_{2,1}(k) & H_{2,2}(k) & \cdots & H_{2,N_t}(k) \\ \vdots & \vdots & \ddots & \vdots \\ H_{N_r,1}(k) & H_{N_r,2}(k) & \cdots & H_{N_r,N_t}(k) \end{bmatrix},$$

where  $H_{i,j}(k)$  denotes the channel gain between the  $j^{th}$  transmit antenna and  $i^{th}$  receive antenna for the  $k^{th}$  subcarrier. Assuming CSI is known at the receiver. The joint antenna and subcarrier selection can be performed at the receiver and only the indices of the selected antennas are fed back to the transmitter so to reduce feedback overhead. If adaptive power allocation is employed, extra data are required in the feedback to provide power allocation information to the transmitter. In the sequel, it is assumed that coherence time of the channel is large enough for accurate CSI to be fed back to the transmitter.

The transmit antenna selection is performed subcarrier by subcarrier to select  $M_t(k)$  transmit antennas out of  $N_t$  transmit antennas for the  $k^{th}$  subcarrier, where  $M_t(k) \leq N_t$  is assumed to avoid rank deficiency when linear receiver is employed. Hence, there are  $M_t(k)$  data streams transmitted on the  $k^{th}$  subcarrier. This selection can be done by precoding the transmit data stream by an  $N_t \times M_t(k)$  precoding matrix,  $\mathbf{W}_{M_t(k),n(k)}$ ,

which is created by choosing  $M_t(k) = 0, 1, \dots, \min(N_t, N_r)$  columns from  $\mathbf{I}_{N_t}$ . Therefore, there are  $N_m \triangleq \min(N_t, N_r) + 1$  number of selection modes for each subcarrier.  $n(k) = 0, 1, \dots, \binom{N_t}{M_t(k)} - 1$  is the index for the data stream-to-antenna mapping for each selection mode. Thus, the precoder is used to map the data stream to specific antennas prior to transmission. Furthermore,  $\mathcal{W}_{M_t(k)} = \left\{ \mathbf{W}_{M_t(k),0}, \mathbf{W}_{M_t(k),1}, \dots, \mathbf{W}_{M_t(k), \binom{N_t}{M_t(k)} - 1} \right\}$  denotes the set containing the  $\binom{N_t}{M_t(k)}$  precoding matrices, with  $\mathbf{W}_{M_t(k),n(k)}$  denoting the  $n(k)^{th}$  precoding matrix in  $\mathcal{W}_{M_t(k)}$ . For  $M_t(k) = 0$ , we further define  $\mathcal{W}_0 = \{\mathbf{W}_{0,0}\}$ , where  $\mathbf{W}_{0,0}$  denotes an empty matrix, which implies no transmission for the specified  $k^{th}$  subcarrier.

Using the precoding matrix, the effective channel matrix is  $\mathbf{H}_p(k) \triangleq \mathbf{H}(k)\mathbf{W}_{M_t(k),n(k)}$  so that the  $N_r \times 1$  received signal vector  $\mathbf{y}(k)$  for the  $k^{th}$  subcarrier can be written as

$$\mathbf{y}(k) = \mathbf{H}_p(k)\sqrt{\mathbf{A}(k)}\mathbf{x}(k) + \mathbf{v}(k),$$

where  $\mathbf{x}(k)$  is an  $M_t(k) \times 1$  transmit signal vector. The constellation size is normalized such that  $E[\mathbf{x}(k)\mathbf{x}^H(k)] = \mathbf{I}_{M_t(k)}$ .  $\mathbf{v}(k)$  is the  $N_r \times 1$  zero-mean complex Gaussian noise vector with variance  $N_0$  for the  $k^{th}$  subcarrier with elements  $v(k)$  that are independent, and identically distributed (i.i.d.). Note that  $\mathbf{v}(k)$  is independently generated for every subcarrier.  $\mathbf{A}(k)$  is an  $M_t(k) \times M_t(k)$  diagonal power allocation matrix, where  $[\mathbf{A}(k)]_{ii}$  denotes the average symbol energy at the  $i^{th}$  transmit antenna for the  $k^{th}$  subcarrier for the duration of one OFDM symbol. This will be elaborated further in the next section as part of the precoder design. The estimated signal  $\hat{\mathbf{x}}(k)$  at the receiver can be written as

$$\hat{\mathbf{x}}(k) = \mathbf{G}_p(k)\mathbf{y}(k) = \sqrt{\mathbf{A}(k)}\mathbf{x}(k) + \mathbf{H}_p^\dagger(k)\mathbf{v}(k), \quad (4.1)$$

where  $\mathbf{G}_p(k)$  denotes the equalization matrix. In the case of ZF equalizer (ZFE),  $\mathbf{G}_p(k) = \mathbf{H}_p^\dagger(k)$ .



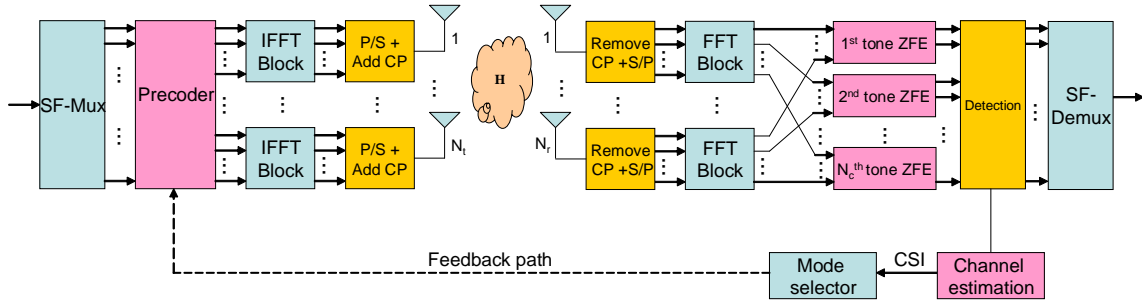


Figure 4.1: Block diagram of proposed multimode precoding scheme.

## 4.3 Proposed Multimode Precoding Scheme

### 4.3.1 Precoder Design

In the present scheme, the precoding matrix  $\mathbf{W}_{M_t(k),n(k)}$  is designed to minimize the average error probability under a constant rate constraint. Specifically, the optimal values of  $M_t(k)$  and  $n(k)$ , denoted as  $M_t^*(k)$  and  $n^*(k)$  henceforth, are determined at the receiver and sent back to the transmitter as precoding parameters via the feedback channel as shown in Figure 4.1. The bitstream at the transmitter is converted to multiple data streams by the spatial-frequency multiplexer (SF-Mux). All the data streams are mapped to transmit antennas according to the precoding parameters and transmitted over the wireless channel after OFDM modulation. At the receiver, the received signal will be equalized with per-tone ZFEs corresponding to the antenna selection at the transmitter. The equalized data streams will then pass through the symbol detector and converted to bitstream with the spatial-frequency demultiplexer (SF-Demux).

For  $M$ -QAM constellation with Gray coding employed for all the data streams, the

BER expression of the  $i^{\text{th}}$  data stream for the  $k^{\text{th}}$  subcarrier can be approximated as [10,33]

$$\begin{aligned}
 P_{b_i}(\mathbf{W}_{M_t(k),n(k)}) &\approx \frac{\sqrt{M-1}}{\sqrt{M} \log_2 \sqrt{M}} \operatorname{erfc} \left( \sqrt{\operatorname{SNR}_i(k) \frac{3\eta}{2(M-1)}} \right) \\
 &= \frac{\sqrt{M-1}}{\sqrt{M} \log_2 \sqrt{M}} \operatorname{erfc} \left( \sqrt{\frac{[\mathbf{A}(k)]_{ii}}{N_0 [(\mathbf{H}_p^H(k) \mathbf{H}_p(k))^{-1}]_{ii}} \frac{3\eta}{2(M-1)}} \right),
 \end{aligned} \tag{4.2}$$

where  $\operatorname{erfc}(\cdot)$  is the complementary error function and  $\operatorname{SNR}_i(k)$  denotes the (post-processing) SNR of the  $i^{\text{th}}$  data stream for the  $k^{\text{th}}$  subcarrier at the output of the ZFE, which can be obtained from (4.1). The post-processing SNR is the parameter of interest in (4.2) because the channel noise is colored by the ZFE, and thus, the noise power can vary as a function of the channel [34]. Therefore, the average BER expression for MIMO-OFDM based systems with precoding and linear equalization can be written as

$$\begin{aligned}
 \bar{P}_b(\bar{\mathbf{W}}) &= \frac{1}{\alpha} \sum_{k=1}^{N_c} \sum_{i=1}^{M_t(k)} P_{b_i}(\mathbf{W}_{M_t(k),n(k)}) \\
 &= \frac{\sqrt{M-1}}{\alpha \sqrt{M} \log_2 \sqrt{M}} \sum_{k=1}^{N_c} \sum_{i=1}^{M_t(k)} \operatorname{erfc} \left( \sqrt{\frac{[\mathbf{A}(k)]_{ii}}{N_0 [(\mathbf{H}_p^H(k) \mathbf{H}_p(k))^{-1}]_{ii}} \frac{3\eta}{2(M-1)}} \right),
 \end{aligned} \tag{4.3}$$

where

$$\bar{\mathbf{W}} = \left[ \mathbf{W}_{M_t(1),n(1)} \quad \mathbf{W}_{M_t(2),n(2)} \quad \cdots \quad \mathbf{W}_{M_t(N_c),n(N_c)} \right],$$

which contains all the precoding matrices specified for the corresponding subcarriers,<sup>2</sup> and  $\alpha = \sum_{k=1}^{N_c} M_t(k)$  denotes the total number of data streams at the transmitter. In addition, the total transmission rate for the multimode scheme is

$$b_T = \alpha \log_2(M) = \sum_{k=1}^{N_c} M_t(k) \log_2(M), \tag{4.4}$$

<sup>2</sup>Even though  $\bar{P}_b(\bar{\mathbf{W}})$  is not explicitly a function of  $\bar{\mathbf{W}}$ ,  $\bar{\mathbf{W}}$  is used here for ease of presentation. The expression is correct in the sense that  $\bar{P}_b$  is a function of all (non-overlapping) submatrices making up  $\bar{\mathbf{W}}$ .

which is used as the rate constraint in the proposed formulation.

From (4.3), it is clear the elements of the power allocation matrix  $[\mathbf{A}(k)]_{ii}$  play an significant role in determining the BER. An obvious choice is to use equal power allocation so that  $[\mathbf{A}(k)]_{ii} = E_b \log_2(M)$ , where  $E_b$  denotes the energy per transmitted bit. From (4.3), the average BER using equal power allocation can be written as

$$\bar{P}_{b,\text{MMEP}}(\bar{\mathbf{W}}) = \frac{\sqrt{M} - 1}{\alpha \sqrt{M} \log_2 \sqrt{M}} \sum_{k=1}^{N_c} \sum_{i=1}^{M_t(k)} \text{erfc} \left( \sqrt{\frac{E_b}{N_0 \left[ (\mathbf{H}_p^H(k) \mathbf{H}_p(k))^{-1} \right]_{ii}} \frac{3 \log_2(M) \eta}{2(M-1)}} \right)$$

and the BER optimized multimode equal power (MMEP) precoder  $\mathbf{W}_{M_t^*(k), n^*(k)}^{(\text{MMEP})}$  for all  $k$  can be obtained by solving

$$\begin{aligned} & \min_{\bar{\mathbf{W}}} \bar{P}_{b,\text{MMEP}}(\bar{\mathbf{W}}) \\ & s.t. \quad b_T = \sum_{k=1}^{N_c} M_t(k) \log_2(M), \\ & \quad 0 \leq M_t(k) \leq N_m - 1, \forall k, 0 \leq n(k) \leq \binom{N_t}{M_t(k)} - 1, \forall k. \end{aligned} \quad (4.5)$$

If  $\mathbf{W}_{M_t^*(k), n^*(k)}^{(\text{MMEP})} = \mathbf{W}_{0,0}$  for a specific  $k$ , none of the antenna will be selected for transmission on that particular  $k^{\text{th}}$  subcarrier. In this case, the BER for this  $k^{\text{th}}$  subcarrier is equal to 0.

To further enhance BER performance, the low complexity inverse power allocation scheme in [35] is also considered. The amount of power allocated in this scheme is inversely proportional to the channel gains such that selected attenuated subcarriers are compensated; thereby boosting BER performance. In other words,  $[\mathbf{A}(k)]_{ii}$  is proportional to  $\left[ (\mathbf{H}_p^H(k) \mathbf{H}_p(k))^{-1} \right]_{ii}$  such that the post-processing SNR of all the data streams for all subcarriers are equalized. Consequently,

$$[\mathbf{A}(k)]_{ii} = \frac{\left[ (\mathbf{H}_p^H(k) \mathbf{H}_p(k))^{-1} \right]_{ii} E_b b_T}{\sum_{k=1}^{N_c} \sum_{i=1}^{M_t(k)} \left[ (\mathbf{H}_p^H(k) \mathbf{H}_p(k))^{-1} \right]_{ii}}, \quad (4.6)$$

where  $E_b b_T$  denotes the total transmitted power. Substituting (4.6) into (4.3), the average BER using inverse power allocation can be written as

$$\bar{P}_{b,\text{MMIP}}(\bar{\mathbf{W}}) = \frac{\sqrt{M} - 1}{\sqrt{M} \log_2 \sqrt{M}} \times \text{erfc} \left( \sqrt{\frac{E_b b_T}{N_0 \sum_{k=1}^{N_c} \sum_{i=1}^{M_t(k)} \left[ (\mathbf{H}_p^H(k) \mathbf{H}_p(k))^{-1} \right]_{ii}} \frac{3\eta}{2(M-1)}}} \right),$$

and the BER optimized multimode inverse power (MMIP) precoder  $\mathbf{W}_{M_t^*(k), n^*(k)}^{(\text{MMIP})}$  for all  $k$  can be obtained by solving

$$\begin{aligned} & \min_{\bar{\mathbf{W}}} \bar{P}_{b,\text{MMIP}}(\bar{\mathbf{W}}) \\ & \text{s.t. } b_T = \sum_{k=1}^{N_c} M_t(k) \log_2(M), \\ & 0 \leq M_t(k) \leq N_m - 1, \forall k, 0 \leq n(k) \leq \binom{N_t}{M_t(k)} - 1, \forall k. \end{aligned} \quad (4.7)$$

Note that  $\sum_{i=1}^{M_t(k)} \left[ (\mathbf{H}_p^H(k) \mathbf{H}_p(k))^{-1} \right]_{ii} = \text{tr} \left( (\mathbf{H}_p^H(k) \mathbf{H}_p(k))^{-1} \right) = \sum_{i=1}^{M_t(k)} \sigma_i^{-2}(\mathbf{H}_p(k))$ . Also, it is easy to see that minimizing  $\sum_{k=1}^{N_c} \sum_{i=1}^{M_t(k)} \sigma_i^{-2}(\mathbf{H}_p(k))$  is equivalent to minimizing the objective function in (4.7). Therefore,  $\mathbf{W}_{M_t^*(k), n^*(k)}^{(\text{MMIP})}$  for all  $k$  can also be obtained by solving

$$\begin{aligned} & \min_{\bar{\mathbf{W}}} \sum_{k=1}^{N_c} \sum_{i=1}^{M_t(k)} \sigma_i^{-2}(\mathbf{H}(k) \mathbf{W}_{M_t(k), n(k)}) \\ & \text{s.t. } b_T = \sum_{k=1}^{N_c} M_t(k) \log_2(M), \\ & 0 \leq M_t(k) \leq N_m - 1, \forall k, 0 \leq n(k) \leq \binom{N_t}{M_t(k)} - 1, \forall k. \end{aligned} \quad (4.8)$$

### 4.3.2 Computation of the Precoders

Since  $\bar{\mathbf{W}}$  contains all the precoding matrices that will determine the transmission rate for each of the corresponding subcarrier, (4.5) and (4.8) become a nonlinear, discrete

constrained minimization problem. If exhaustive search is employed, the number of points to be searched for (4.5) and (4.8) is  $\left[ \sum_{i=0}^{N_m-1} \binom{N_t}{i} \right]^{N_c}$ ; making this method infeasible because, in practice,  $N_c$  can be in the order of  $10^3$ . To bypass this problem, Lagrangian relaxation [20, p. 323] can be used to obtain a near-optimal solution.

Since  $\bar{P}_{b,\text{MMEP}}(\bar{\mathbf{W}})$  and  $\bar{P}_{b,\text{MMIP}}(\bar{\mathbf{W}})$  (or equivalently  $\sum_{k=1}^{N_c} \sum_{i=1}^{M_t(k)} \sigma_i^{-2}(\mathbf{H}_p(k))$ ) are functions of  $\mathbf{H}_p(k)$ , they can be written more generally as  $\sum_{k=1}^{N_c} f(\mathbf{H}(k)\mathbf{W}_{M_t(k),n(k)})$ , such that the Lagrangian relaxation of (4.5) and (4.8), with respect to the rate constraint, can be written as

$$\ell_{LR}(\lambda) = \min_{\bar{\mathbf{W}}} \ell(\bar{\mathbf{W}}, \lambda), \quad \lambda \in \mathbb{R}_+, \quad (4.9)$$

where

$$\begin{aligned} \ell(\bar{\mathbf{W}}, \lambda) &= \sum_{k=1}^{N_c} f_k(\mathbf{H}(k)\mathbf{W}_{M_t(k),n(k)}) + \lambda \left( N_c M_t - \sum_{k=1}^{N_c} M_t(k) \right) \\ &= \sum_{k=1}^{N_c} f(\mathbf{H}(k)\mathbf{W}_{M_t(k),n(k)}) + \lambda (M_t - M_t(k)) \\ &= \sum_{k=1}^{N_c} \ell_k(\mathbf{W}_{M_t(k),n(k)}, \lambda) \end{aligned} \quad (4.10)$$

is the Lagrangian and  $\lambda$  is the Lagrange multiplier. Note that  $\ell_k(\mathbf{W}_{M_t(k),n(k)}, \lambda)$  can be regarded as the Lagrangian for the  $k^{\text{th}}$  subcarrier. It can be observed that  $\ell_k(\mathbf{W}_{M_t(k),n(k)}, \lambda)$  is independently additive since each subcarrier is orthogonal to each other. As a result, the minima of  $\ell(\bar{\mathbf{W}}, \lambda)$  is obtained when  $\ell_k(\mathbf{W}_{M_t(k),n(k)}, \lambda)$  is minimized for each  $k$ . Furthermore, the Lagrangian for all subcarriers share the same parameter  $\lambda$ . Hence, once  $\lambda$  is known,  $\bar{\mathbf{W}}$  can be determined by considering  $\mathbf{W}_{M_t(k),n(k)}$  which minimizes  $\ell_k(\mathbf{W}_{M_t(k),n(k)}, \lambda)$ .

From [20, p. 324], the Lagrangian dual function is  $\ell_{LD} = \max_{\lambda \geq 0} \ell_{LR}(\lambda)$ , where  $\ell_{LD}$  is the infimum of the objective function in (4.5) and (4.8) and it is a convex function [36, p. 215]. Thus, the global optimal solution for  $\ell_{LD}$  can always be attained efficiently. Since  $\ell_{LR}(\lambda)$  is a piecewise linear and convex function of  $\lambda$ ,  $\ell_{LD}$  can be solved using the

subgradient algorithm [20, p. 409]. Furthermore, such a solution can be refined by the branch and bound algorithm [20, p. 355] to obtain a better solution.

The subgradient algorithm can easily be implemented using the bisection method to obtain the solution efficiently because  $\lambda$  is a scalar. Although the derivation of  $\overline{\mathbf{W}}$  which minimizes  $\ell(\overline{\mathbf{W}}, \lambda)$  can be simplified by solving each  $\mathbf{W}_{M_t(k), n(k)}$  that minimizes  $\ell_k(\mathbf{W}_{M_t(k), n(k)}, \lambda)$  for a given  $\lambda$  exhaustively, it may be infeasible as there are  $\sum_{i=0}^{N_m-1} \binom{N_t}{i}$  possible solutions for each subcarrier.

A preselecting procedure can be employed as an alternative to reduce the search region such that there are only  $N_m$  possible solutions for each subcarrier. This is done by first obtaining  $\mathbf{W}_{M_t(k), n^*(k)}$  for each selection mode. The optimal precoder  $\mathbf{W}_{M_t^*(k), n^*(k)}$  for each  $k$  can thus be solved using the Lagrangian relaxation method. This reduces the total number of precoding matrices being evaluated in each iteration to  $N_c N_m$ .

## 4.4 Unimode Precoding

In order to compare and appreciate the performance gain obtained from the proposed multimode precoding scheme, the unimode precoding scheme is also derived. Unlike the proposed multimode scheme, the number of antennas is assumed to be a priori known (hence, it is no longer a design parameter) and it is uniform across all subcarriers, i.e.  $M_t(k) = M_t$ . Hence, only the data stream-to-antenna mapping needs to be determined. In order to compare the proposed multimode and unimode scheme in a fair manner,  $M_t$  should be chosen such that  $N_c M_t = \sum_{k=1}^{N_c} M_t(k)$  is satisfied. Defining

$\mathcal{W}_{M_t} = \left\{ \mathbf{W}_{M_t,0}, \mathbf{W}_{M_t,1}, \dots, \mathbf{W}_{M_t, \binom{N_t}{M_t} - 1} \right\}$  as the set containing the precoding matrices  $\mathbf{W}_{M_t, n(k)}$ , for  $n(k) = 0, 1, \dots, \binom{N_t}{M_t} - 1$ , which are created by choosing  $M_t$  columns from  $\mathbf{I}_{N_t}$  for all  $k$ . Following similar derivation as in Section 4.3, the average BER for unimode

precoding can then be written as

$$\begin{aligned}\bar{P}_{b,\text{UMEP}}(\bar{\mathbf{W}}) &= \frac{1}{N_c M_t} \sum_{k=1}^{N_c} \sum_{i=1}^{M_t} P_{b_i}(\mathbf{W}_{M_t,n(k)}) \\ &= \frac{1}{N_c} \sum_{k=1}^{N_c} P_{b_{\text{avg}}}(\mathbf{W}_{M_t,n(k)}),\end{aligned}\tag{4.11}$$

where  $P_{b_{\text{avg}}}(\mathbf{W}_{M_t,n(k)}) \triangleq \frac{1}{M_t} \sum_{i=1}^{M_t} P_{b_i}(\mathbf{W}_{M_t,n(k)})$  is the average BER for the  $k^{\text{th}}$  subcarrier. Obviously, to minimize  $\bar{P}_b(\bar{\mathbf{W}})$  in (4.11) is equivalent to minimize  $P_{b_{\text{avg}}}(\mathbf{W}_{M_t,n(k)})$  for each subcarrier. From (4.2), the average BER for the  $k^{\text{th}}$  subcarrier using equal power allocation can be written as

$$P_{b_{\text{avg}}}^{(\text{UMEP})}(\mathbf{W}_{M_t,n(k)}) = \frac{\sqrt{M} - 1}{M_t \sqrt{M} \log_2 \sqrt{M}} \times \sum_{i=1}^{M_t} \text{erfc} \left( \sqrt{\frac{E_b}{N_0 \left[ (\mathbf{H}_p^H(k) \mathbf{H}_p(k))^{-1} \right]_{ii}} \frac{3\eta \log_2 M}{2(M-1)}} \right),$$

and the BER optimized unimode equal power (UMEP) precoder for each subcarrier is

$$\mathbf{W}_{M_t,n^*(k)}^{(\text{UMEP})} = \arg \min_{\mathbf{W}_{M_t,n(k)} \in \mathcal{W}_{M_t}} P_{b_{\text{avg}}}^{(\text{UMEP})}(\mathbf{W}_{M_t,n(k)}).$$

Similarly, the average BER using inverse power allocation can be written as

$$\bar{P}_{b,\text{UMIP}}(\bar{\mathbf{W}}) = \frac{\sqrt{M} - 1}{\sqrt{M} \log_2 \sqrt{M}} \times \text{erfc} \left( \sqrt{\frac{E_b b_T}{N_0 \sum_{k=1}^{N_c} \sum_{i=1}^{M_t} \left[ (\mathbf{H}_p^H(k) \mathbf{H}_p(k))^{-1} \right]_{ii}} \frac{3\eta}{2(M-1)}} \right).$$

It is obvious that minimizing  $\bar{P}_{b,\text{UMIP}}(\bar{\mathbf{W}})$  is equivalent to minimizing

$\sum_{k=1}^{N_c} \sum_{i=1}^{M_t} \left[ (\mathbf{H}_p^H(k) \mathbf{H}_p(k))^{-1} \right]_{ii}$  for each subcarrier. Hence, the BER optimized unimode inverse power (UMIP) precoder for each subcarrier is

$$\mathbf{W}_{M_t,n^*(k)}^{(\text{UMIP})} = \arg \min_{\mathbf{W}_{M_t,n(k)} \in \mathcal{W}_{M_t}} \sum_{i=1}^{M_t} \sigma_i^{-2}(\mathbf{H}_p(k)).$$

## 4.5 Complexity Analysis

The computational complexity under consideration is defined as the number of multiplications and additions, which is identical to the definition of *flop* as indicated in [37, p.18].

The computational complexity for the MMEP, MMIP, UMEP, UMIP schemes, and the MIMO-OFDM implementation of the selection criterion 5 (SC5) method in [3] is summarized in Table 4.1.

The computational complexity for the proposed multimode scheme can be considered in two stages. The first stage involves the computation of  $f(\mathbf{H}(k)\mathbf{W}_{M_t(k),n(k)})$  for all combinations of  $M_t(k)$  and  $n(k)$ , while the second stage considers the use of the Lagrangian relaxation method to attain  $\mathbf{W}_{M_t^*(k),n^*(k)}$ .<sup>3</sup>

It is clear that there are a total of  $N_c \sum_{i=1}^{N_m-1} \binom{N_t}{i}$  effective channel matrices which need to be evaluated. Assuming that the  $R$ -SVD algorithm [37, p. 253] is employed to compute all inverses and singular values. In the case of the MMEP precoder, evaluating  $f(\mathbf{H}(k)\mathbf{W}_{M_t(k),n(k)})$  is equivalent to evaluating  $(\mathbf{H}_p^H(k)\mathbf{H}_p(k))^{-1}$  which also equals to  $\mathbf{V}^H(k)\mathbf{\Sigma}^{-2}(k)\mathbf{V}(k)$ , where  $\mathbf{V}(k)$  and  $\mathbf{\Sigma}(k)$  are the singular vector and value matrices of  $\mathbf{H}_p(k)$ , respectively. Hence, the amount of computation required will be  $\left( N_c \sum_{i=1}^{N_m-1} \binom{N_t}{i} (2N_r i^2 + 11i^3) \right)$ . For the MMIP precoder, evaluating  $f(\mathbf{H}(k)\mathbf{W}_{M_t(k),n(k)})$  is equivalent to evaluating  $\sigma_i^{-2}(\mathbf{H}_p(k))$ . Hence, the amount of computation required will be  $\left( N_c \sum_{i=1}^{N_m-1} \binom{N_t}{i} (2N_r i^2 + 2i^3) \right)$ . In the second stage, the evaluation of the Lagrangian relaxation is considered in two parts. The first part considers the computation of  $\lambda$  using the bisection method and the second considers the evaluation of the Lagrangian.

The bisection method begins by defining an interval  $(0, \lambda^{\max})$ , where  $\lambda^{\max}$  is initiated to be 1. It is subsequently increased (by doubling it) until  $\sum_{k=1}^{N_c} M_t(k) > N_c M_t$ . The bisection method will then be applied to decrease  $\lambda$  until the rate constraint is tight, whereby the optimum  $\lambda$ , denoted as  $\lambda^*$ , is obtained. Assuming that a precision of  $\epsilon_\lambda$

---

<sup>3</sup>Since the most computational expensive part in the first stage is to compute  $(\mathbf{H}_p^H(k)\mathbf{H}_p(k))^{-1}$  for equal power allocation scheme or  $\sigma_i^{-2}(\mathbf{H}_p(k))$  for inverse power allocation scheme, the computation of the operations, such as  $\text{erfc}(\cdot)$ ,  $\sqrt{\cdot}$ , etc, is therefore omitted.



is used in obtaining  $\lambda^*$  and the computations for attaining a suitable  $\lambda^{\max}$  is negligible, then the number of iterations for the bisection method will be  $\log_2\left(\frac{1}{\epsilon_\lambda}\right)$  [38]. For each iteration, 1 multiplication and 1 addition will be used for the computation of  $\lambda$  using the bisection method. For the second part of the second stage, if the preselection procedure is not used, then  $\ell_k(\mathbf{W}_{M_t(k),n(k)}, \lambda)$  will need to be evaluated  $N_c \sum_{i=0}^{N_m-1} \binom{N_t}{i}$  times in computing the Lagrangian relaxation. If preselection procedure is employed, then only  $\ell_k(\mathbf{W}_{M_t(k),n^*(k)}, \lambda)$  needs to be evaluated. This, however, only needs to be performed  $N_c N_m$  times as described in Section 4.3.2. Assuming  $f(\mathbf{H}(k)\mathbf{W}_{M_t(k),n(k)})$  has been calculated in the first stage, 1 multiplication and 2 additions are required to compute one  $\ell_k(\mathbf{W}_{M_t(k),n(k)}, \lambda)$  in (4.10). Since the preselection procedure will only be performed before bisection method, the computation is relatively small compared to that of the Lagrangian. Thus, the computation for the preselection procedure can be ignored. The total number of computations for the second stage will then be  $\log_2\left(\frac{1}{\epsilon_\lambda}\right)(2 + 3N_c N_m)$ .

For the unimode scheme, each subcarrier requires calculation of  $f(\mathbf{H}(k)\mathbf{W}_{M_t,n(k)})$  for all  $n(k)$ . If UMIP is employed, evaluating  $f(\mathbf{H}(k)\mathbf{W}_{M_t,n(k)})$  involves computing  $\sigma_i^{-2}(\mathbf{H}_p(k))$ . Using the  $R$ -SVD algorithm, the computational complexity will be  $N_c \binom{N_t}{M_t} (2N_r M_t^2 + 2M_t^3)$ . In comparison, if UMEP is employed, evaluating  $f(\mathbf{H}(k)\mathbf{W}_{M_t,n(k)})$  involves computing  $(\mathbf{H}_p^H(k)\mathbf{H}_p(k))^{-1} = \mathbf{V}^H(k)\mathbf{\Sigma}^{-2}(k)\mathbf{V}(k)$ . Hence, the computational complexity will be  $N_c \binom{N_t}{M_t} (2N_r M_t^2 + 11M_t^3)$ .

From the above, it is clear that the computational burden lies in the evaluation of  $f(\mathbf{H}(k)\mathbf{W}_{M_t,n(k)})$ , which increases as the number of selection modes are increased, as in the proposed multimode scheme. However, the complexity will not be too high when  $N_m$  is small.

Table 4.1: Number of multiplications and additions for the proposed multimode precoding schemes, the unimode precoding scheme in Section 4.4, and an MIMO-OFDM implementation of the SC5 scheme in [3].

Scheme	$f(\mathbf{H}(k)\mathbf{W}_{M_t(k),n(k)})$	Stage 1	Stage 2 (with preselection)
MMEP	$(\mathbf{H}_p^H(k)\mathbf{H}_p(k))^{-1} = \mathbf{V}^H(k)\mathbf{\Sigma}^{-2}(k)\mathbf{V}(k)$	$N_c \sum_{i=1}^{N_m-1} \binom{N_t}{i} (2N_r i^2 + 11i^3)$	$\log_2\left(\frac{1}{\epsilon_\lambda}\right) (2 + 3N_c N_m)$
MMIP	$\sigma_i^{-2}(\mathbf{H}_p(k))$	$N_c \sum_{i=1}^{N_m-1} \binom{N_t}{i} (2N_r i^2 + 2i^3)$	$\log_2\left(\frac{1}{\epsilon_\lambda}\right) (2 + 3N_c N_m)$
UMEP	$(\mathbf{H}_p^H(k)\mathbf{H}_p(k))^{-1} = \mathbf{V}^H(k)\mathbf{\Sigma}^{-2}(k)\mathbf{V}(k)$	$N_c \binom{N_t}{M_t} (2N_r M_t^2 + 11M_t^3)$	—
UMIP	$\sigma_i^{-2}(\mathbf{H}_p(k))$	$N_c \binom{N_t}{M_t} (2N_r M_t^2 + 2M_t^3)$	—
SC5 [3]	$(\mathbf{H}_p^H(k)\mathbf{H}_p(k))^{-1} = \mathbf{V}^H(k)\mathbf{\Sigma}^{-2}(k)\mathbf{V}(k)$	$N_c \sum_{i=1}^{N_m-1} \binom{N_t}{i} (2N_r i^2 + 11i^3)$	—

## 4.6 Simulation Results and Discussions

In all simulations,  $N_c = 64$  and  $N_{cp} = 16$ . In this case,  $\eta = 0.8$ . It is assumed that the transmission is ISI- and ICI-free. The channel coefficients are directly generated independently in the frequency domain with a Rayleigh distribution, where the fading process is normalized such that  $E[|H_{i,j}(k)|^2] = 1$ .

The BER performance for the MMEP, MMIP, UMEP, and UMIP precoding schemes are shown in Figure 4.2 with spectral efficiency  $R = M_t \log_2(M) = 4$  bits/s/Hz and  $M_t = 2$ . The constellation is chosen such that the transmission rate constraint in (4.4) is satisfied. In the following,  $X \times Y$  denotes MIMO-OFDM based spatial multiplexing systems with  $X$  transmit and  $Y$  receive antennas.  $3 \times 3$ , and  $4 \times 4$  systems are considered. In addition,  $1 \times 1$  and  $2 \times 2$  systems with no precoding (no diversity) are also plotted for comparison. In this instance, equal power (EP) allocation is used. From Figure 4.2, all precoding schemes can achieve lower BER than  $1 \times 1$  and  $2 \times 2$  systems as they do not benefit from any selection diversity. For the  $3 \times 3$  system, the proposed MMEP

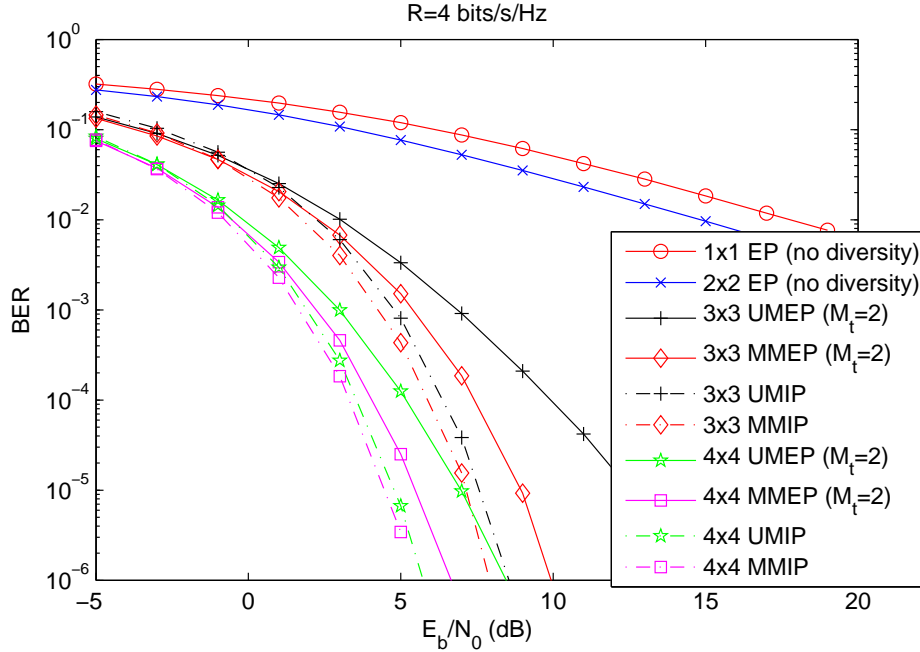


Figure 4.2: BER vs. SNR performance for multimode and unimode schemes ( $R = 4$  bits/s/Hz).

precoding scheme outperforms the UMEP precoding scheme by 1.5 dB at a BER of  $10^{-3}$ . This is possible because channel gain diversity is exploited in the MMEP scheme. Moreover, the MMIP precoding method outperforms the MMEP precoding method, and the UMIP scheme outperforms the UMEP scheme. For  $3 \times 3$  system, the proposed MMIP scheme outperforms UMEP scheme by 2.7 dB at a BER of  $10^{-3}$ . It is interesting to note that in the  $4 \times 4$  system, the performance gains of all the proposed multimode schemes over their unimode counterparts are less than those in  $3 \times 3$  system. This is because the extra antenna pair increases the spatial diversity, hence, the unimode schemes can directly benefit from extra selection diversity to select antenna subset of good quality without exploiting the diversity over all the subcarriers. Furthermore, the performance gap between MMIP/UMIP is less than that of MMEP/UMEP. This is because the inverse power allocation scheme reduces the diversity of the post-processing gains over all the subcarriers by compensating the attenuated subcarriers.

The BER performances for various precoding schemes in a  $4 \times 4$  system with spectral efficiency  $R = M_t \log_2(M) = 12$  bits/s/Hz and  $M_t = 3$  are shown in Figure 4.3. In addition to the unimode scheme, SC1 scheme in [2] and the SC5 in [3] are also included. Since SC1 and SC5 were originally proposed for MIMO spatial multiplexing systems, an MIMO-OFDM implementation of the two schemes are used here. SC1 is an unimode scheme where an optimal antenna subset is selected based on the maximum minimum post-processing SNR. SC5 is a multimode scheme in which the optimal modes for  $M_t$  and  $M$ -QAM pair are chosen. Note that this is different from the present multimode scheme that employs uniform constellation and adaptively changes the number of transmit antennas. In the simulation,  $(M_t, M) = (2, 64)$  and  $(3, 16)$  are used to achieve 12 bits/s/Hz spectrum efficiency for each subcarrier. From the figure, the proposed MMEP and MMIP precoding schemes clearly outperform all the other competing schemes. This shows that BER performance can be improved by exploiting channel gain diversity in frequency-selective fading channels. However, this performance gain comes at the cost of extra feedback information from the receiver as the amount of power allocated for each data stream needs to be transmitted. Therefore, the performance of inverse power allocation based precoders are expected to be more sensitive to inaccuracy or delay in the CSI feedback.



Figure 4.3: BER vs. SNR performance between multimode, unimode, SC1 [2], and SC5 [3] schemes ( $R = 12$  bits/s/Hz).

# Chapter 5

## Conclusions and Future Works

### 5.1 Conclusions

In this thesis, we proposed resource allocation techniques for wireless multimedia communications. The CLDOSSA is an OFDM-based algorithm can easily achieve fine-grained UEP levels protect video content of different importance. Moreover, it can be implemented without exact CSI feedback. For the cross-layer optimization of the proposed scheme, we jointly optimized the configuration in the physical layer and link layer and solved for the number of selected subcarriers employed in the CLDOSSA for each slice with Lagrangian relaxation method. Simulation results show that the proposed scheme can outperform the UEP OSSA, EEP OSSA, and the EEP implementation of [1] in terms of PSNR, especially at low SNR.

In addition, a multimode antenna precoding scheme was also proposed for MIMO-OFDM based spatial muxltiplexing systems. Simulation results show that the proposed schemes can exploit spatial diversity as well as channel gain diversity to enhance link reliability. Furthermore, the inverse power allocation strategy simplifies the precoder design compared to that of the equal power since only the eigenmodes of the effective channel matrix are used. Although the inverse power allocation based precoders outperform other

schemes, this gain comes at the cost of extra feedback information from the receiver as exact channel gain for each subcarrier needs to be transmitted.

## 5.2 Future Works

In the future, we can further investigate video streaming using the DLDOSSA in a multiple user scenario, where the transmit rate balancing among all the users will be a crucial issue. Moreover, the CLDOSSA can be extended for use in MIMO-OFDM systems to further enhance the transmission rate.

Since all the proposed schemes in this thesis assume CSI is perfectly known at the transmitter, the proposed scheme can allocate the resource to proper subcarriers or transmit antennas and thus elevate the system performance. However, CSI at the transmitter is usually imperfect due to imperfect channel estimation, quantization of CSI, or delay of CSI feedback from the receiver. Therefore, investigation into how these factors can impact system performance is keen in achieving the desirable performance. Furthermore, for the MIMO-OFDM systems, the channel was assumed to be spatially uncorrelated. This is not usually the case for the mobile device as size of the device limits placements of the antennas. Therefore, schemes which also take this factor into account will make the system even more practical.

# Bibliography

- [1] J. Campello, “Optimal discrete bit loading for multicarrier modulation systems,” in *Proc. of the Intl. Symp. Information Theory*, Cambridge, Mass, USA, Aug. 1998, p. 193.
- [2] R.W. Heath, Jr., S. Sandhu, and A. Paulraj, “Antenna selection for spatial multiplexing systems with linear receivers,” *IEEE Communications Letter*, vol. 5(4), pp. 142–144, Apr. 2001.
- [3] R.W. Heath, Jr. and D.J. Love, “Multimode antenna selection for spatial multiplexing systems with linear receivers,” *IEEE Trans. on Signal Processing*, vol. 53(8), pp. 3042–3056, Aug. 2005.
- [4] W. Stallings, *Data and Computer Communications*. Prentice Hall, 2007.
- [5] G.L. Stüber *et al.*, “Broadband MIMO-OFDM wireless communications,” in *Proc. of the IEEE*, vol. 92(2), Feb. 2004, pp. 271–294.
- [6] D. R. Company, *Using MIMO-OFDM technology to boost wireless LAN performance today*. St. Louis: White Paper, 2005.
- [7] G.J. Foschini and M. Gans, “On limits of wireless communications in fading environment when using multiple antennas,” *Wireless Personal Communications*, vol. 6, pp. 311–335.



- [8] L. Zheng and D.N.C. Tse, "Diversity and multiplexing: a fundamental tradeoff in multiple-antenna channels," *IEEE Trans. on Inform. Theory*, vol. 49(5), pp. 1073–1096, May 2003.
- [9] D. Dardari *et al.*, "Layered video transmission on adaptive OFDM wireless Systems," *EURASIP Journal on Applied Signal Processing*, vol. 2004(10), pp. 1557–1567, 2004.
- [10] D. Dardari, "Ordered subcarrier selection algorithm for OFDM-Based high-speed WLANs," *IEEE Trans. on Wireless Communications*, vol. 3(5), pp. 1452–1458, Sept. 2004.
- [11] Z. Wang *et al.*, "Jointly optimized transmission of scalable video streams in OFDM wireless systems," vol. 1, Nov. 2006.
- [12] C.-H. Chen, C.C. Fung and S.-J. Wang, "Packetized video transmission for OFDM wireless systems with dynamic ordered subcarrier selection algorithm," in *Proc. of the Intl. Conf. on Acoustics, Speech, and Signal Processing*, Apr. 2009, pp. 1993–1996.
- [13] ITU-T Rec. H.264/ISO/IEC 11496-10, "Advanced Video Coding," Final Committee Draft, Document JVT-E022, Sep. 2002.
- [14] T. Wiegand *et al.*, "Overview of the H.264/AVC video coding standard," *IEEE Trans. on Circuit and Systems for Video Technology*, vol. 13(7), pp. 560–576, Jul. 2003.
- [15] O. Harmanici and A.M. Tekalp, "Rate-distortion optimal video transport over IP allowing packets with bit errors," *IEEE Trans. on Image Processing*, vol. 16(5), pp. 1315–1326, May 2007.
- [16] S. Wenger and G. Cote, "Using RFC2429 and H.263+ at low to medium bitrates for low latency applications," in *Proc. of the Packet Video Workshop*, Apr. 1999.
- [17] J.G. Proakis, *Digital Communications*. New York: 4th ed. Wiley, 2001.

- [18] D. Dardari and V. Tralli, “High-speed indoor wireless communications at 60 Ghz with coded OFDM,” *IEEE Trans. on Communications*, vol. 47(11), pp. 1709–1721, Nov. 1999.
- [19] H. David, *Order Statistics*. New York: Wiley, 1981.
- [20] G. Nemhauser and L. Wolsey, *Integer and Combinatorial Optimization*. New York: Wiley, 1988.
- [21] D. Gore, R. Nabar, and A. Paulraj, “Selecting an optimal set of transmit antennas for a low rank matrix channel,” in *Proc. of the Intl. Conf. on Acoustics, Speech, and Signal Processing*, vol. 5, Jun. 2000, pp. 2785–2788.
- [22] D. Gore, R. Heath, and, and A. Paulraj, “Statistical antenna selection for spatial multiplexing systems,” in *Proc. of the Intl. Conf. on Communications*, vol. 1, Apr. 2002, pp. 454–454.
- [23] A. Gorokhov, “Antenna selection algorithms for MEA transmission systems,” in *Proc. of the Intl. Conf. on Acoustics, Speech, and Signal Processing*, vol. 3, May 2002, pp. 2857–2860.
- [24] B. Lu, X. Wang, and K.R. Narayanan, “LDPC-based space-time coded OFDM systems over correlated fading channels: performance analysis and receiver design,” *IEEE Trans. on Communications*, vol. 50(1), pp. 74–88, Jan. 2002.
- [25] I. Bahececi, T.M. Duman, and Y. Altunbasak, “Performance of MIMO antenna selection for space-time coded OFDM systems,” in *Proc. of the Wireless Communications and Networking Conference*, vol. 2, Mar. 2004, pp. 987–992.
- [26] M. Collados and A. Gorokhov, “Performance of MIMO-OFDM WLAN systems and antenna subset selection,” in *Proc. of the IEEE Benelux Chapter on communications and Vehicular Technology Symposium*, 2003.

- [27] M. Torabi and M.R. Soleymani, "Adaptive modulation for OFDM systems using space-frequency block codes," in *Proc. of the IEEE Wireless Communications and Networking*, vol. 1, Mar. 2003, pp. 61–65.
- [28] G.L. Stüber *et al.*, "Joint antenna and subcarrier selection for MIMO-OFDM systems," in *Proc. of the IEEE Intl. Conf. Communications, Circuits and Systems*, vol. 2, Jun. 2006, pp. 1153–1156.
- [29] M. Torabi, "Antenna selection for MIMO-OFDM systems," *Signal Processing*, vol. 88(10), pp. 2431–2441, Oct. 2008.
- [30] N. Khaled, S. Thoen, and L. Deneire, "Optimizing the joint transmit and receive MMSE design using mode selection," *IEEE Trans. on Communications*, vol. 53(4), pp. 730–737, Apr. 2005.
- [31] H. Sampath, P. Stoica, and A. Paulraj, "Generalized linear precoder and decoder design for MIMO channels using the weighted MMSE criterion," *IEEE Trans. on Communications*, vol. 49(12), pp. 2198–2206, Dec. 2001.
- [32] A. Scaglione *et al.*, "Optimal designs for space-time linear precoders and decoders," *IEEE Trans. on Signal Processing*, vol. 50(5), pp. 1051–1064, May 2002.
- [33] K. Cho and D. Yoon, "On the general BER expression of one- and two-dimensional amplitude modulations," *IEEE Trans. on Communications*, vol. 50(7), pp. 1074–1080, Jul. 2002.
- [34] R.W. Heath, Jr. and A. Paulraj, "Antenna selection for spatial multiplexing systems based on minimum error rate," in *Proc. of the Intl Conf. on Communications*, vol. 7, Jun. 2001, pp. 2276–2280.
- [35] N.Y. Ermolova and B. Makarevitch, "On subchannel inversion for improvement of power efficiency in OFDM-based systems," *IET Communications*, vol. 3(5), 2007.

- [36] S. Boyd and L. Vandenberghe, *Convex Optimization*. Cambridge University Press, 2004.
- [37] G.H. Golub and C.F. Van Loan, *Matrix Computations*. 3th ed. John Hopkins Press, 1996.
- [38] R. Cendrillon *et al.*, “Autonomous spectrum balancing for digital subscriber lines,” *IEEE Trans. on Signal Processing*, vol. 55(8), pp. 4241–4257, Aug. 2007.

